1   Manuscript Revised with Track Changes to Address Comments from Reviewer #2

2   12/20/10

3

4   # Air-sea Exchange of Dimethylsulfide (DMS) in the Southern

5   Ocean

6   – Measurements from SO GasEx Compared to Temperate and Tropical

7   Regions

8

9   M. Yang[1], B.W. Blomquist[1], C.W. Fairall[2], S.D. Archer[3], B.J. Huebert[1]

10   [1] Department of Oceanography, University of Hawaii, Honolulu, HI, USA

11   [2] NOAA Earth System Research Laboratory, Physical Sciences Division, Boulder, CO, USA

12   [3] Plymouth Marine Laboratory, Prospect Place, Plymouth, PL1 3DH, UK

13

14   Correspondence to: Barry J. Huebert

15   (huebert@hawaii.edu)

16

Abstract

18   Dimethylsulfude (DMS), a biogenic sulfur gas produced in the surface ocean and

19   constantly emitted to the marine atmosphere, has recently emerged as one of the key

20   gases with which to directly quantify the air-sea transfer velocity (k). In the Southern

21   Ocean Gas Exchange Experiment (SO GasEx), we measured atmospheric DMS

22   concentration of 118±54 pptv (1 sigma), DMS sea-to-air flux of 2.9±2.1 μmoles m^{-2} day^{-1}

23   by eddy covariance, and seawater DMS concentration of 1.6±0.7 nM. Dividing flux by

24   the concurrent air-sea concentration difference yields the transfer velocity of DMS

25   (k_{DMS}). Compared to previous open ocean measurements in the equatorial East Pacific,

26   Sargasso Sea, Northeast Atlantic, and Southeast Pacific, k_{DMS} in the Southern Ocean was

27   lower mostly because of the cold surface water. Furthermore, we found that the Schmidt

28   number normalization for waterside diffusivity does not account for all temperature

29   effects in k_{DMS}. Higher solubility of DMS at a lower temperature results in greater airside

30   control and less transfer of the gas by bubbles formed from breaking waves. We present

31   here a normalization of k_{DMS} for the temperature dependence in solubility, in addition to

32   diffusivity. k_{DMS} is separated to interfacial and bubble components. We assume

33   interfacial exchange to be linearly related to the tangential friction velocity and estimate

34   bubble-mediated exchange from the residual, which is a small term for DMS. The final

35   normalized k_{DMS} shows good agreement among the five cruises, and is similar to those of

36   less soluble gases such as carbon dioxide in low-to-moderate winds but significantly

37   lower in high winds.

1. Introduction

Transfer of gases across the air-water interface has profound implications for the carbon and sulfur budgets in the marine atmosphere and biosphere. The sea-to-air transport of dimethylsulfide (DMS) is of particular interest because the gas is thought to influence climate through the production of sulfate aerosols that could serve as cloud condensation nuclei [*Charlson et al.*, 1987]. DMS is derived from phytoplankton in the surface seawater (DMS_w) and typically has a concentration of a few nM. Because of photochemical loss and dilution, the atmospheric DMS concentration (DMS_a) in the boundary layer is orders of magnitude lower than the Henry's Law equilibrium concentration. As a result, the flux of DMS is always positive (upward from the ocean surface) and is the largest natural source of reduced sulfur to the marine atmosphere [*Lovelock et al.*, 1972]. The substantial magnitude of the sea-to-air flux and the absence of other sources make it relatively easy to quantify the DMS transfer velocity (k_{DMS}):

$$k_{DMS} = Flux/(DMS_w - \alpha \cdot DMS_a) \tag{1}$$

Here α is the dimensionless Ostwald solubility of the gas (adopted from *Dacey et al.* [1984] for DMS). The second term inside of the parenthesis represents the waterside DMS concentration that would be in equilibrium with the bulk airside concentration.

Air-sea gas transfer is controlled by molecular and turbulent diffusion on both sides of the interface, with the concentration difference being the driving force for exchange. Close to the interface, turbulent transport diminishes and molecular diffusion dominates. With resistance on both sides of the boundary acting in series, the total transfer velocity of a gas (k) is a function of waterside transfer velocity (k_w) and airside transfer velocity (k_a):

63 $$k = [\frac{1}{k_w} + \frac{\alpha}{k_a}]^{-1}$$ (2)

64 For exchange of sparingly soluble gases, including carbon dioxide (CO_2), sulfur

65 hexafluoride (SF_6), and helium (He), the molecular sub-layer on the waterside provides

66 the greatest resistance. In contrast, exchange of highly soluble gases, such as methanol,

67 is controlled by airside resistance, with water vapor representing complete airside control.

68 DMS is intermediate in solubility, with $\alpha = 14.2$ at 20 °C in seawater.

69   Since transfer velocity of a gas (k) scales inversely to resistance, turbulence

70 generated from wind stress (τ) that thins the molecular sub-layers increases k. Because

71 the 10-meter wind speed (U_{10}) is much easier to measure than τ, most gas exchange

72 parameterizations are based on U_{10} only [*Liss and Merlivat*, 1986; *Wanninkhof*, 1992;

73 *Nightingale et al.*, 2000; *Ho et al.*, 2006]. However these models diverge significantly in

74 high winds. From a more physics-based perspective, *Csanady* [1990] theorized that k has

75 a linear dependence on the friction velocity (u_*), which is related to stress through the

76 density of air (ρ): $\tau = \rho\, u_*^2$. Our direct observations of k_{DMS} and u_* during the DOGEE

77 cruise confirmed this linearity at moderate wind speeds [*Huebert et al.*, 2010]. However,

78 this linear relationship might not hold in calm and heavy breaking wave conditions, when

79 additional physical processes confound this simple picture of shear-driven interfacial

80 exchange. When $U_{10} < 2\sim3$ m s^{-1}, buoyancy-driven free convection at the ocean surface

81 may account for more transfer than wind shear [*Soloviev and Schlüssel*, 1994]. Above

82 7~8 m s^{-1}, whitecaps start to form on the sea surface. The additional surface area from air

83 bubbles [*Woolf*, 1997] and the associated turbulent plume [*Monahan and Spillane*, 1984]

84 can increase gas exchange. Insoluble gases partition more readily into bubbles than

85 soluble gases and should therefore show enhanced transfer in moderate-to-high winds. In

86   contrast, a more soluble gas like DMS exhibits only modest bubble-mediated

87   enhancement for wind speeds up to ~10 m s^{-1} [*Blomquist et al.*, 2006].

88   In the past several years, we have measured the sea-to-air flux of DMS with eddy

89   covariance (EC) on five cruises in distinctively different oceanic environments (Fig. 1).

90   Chronologically, they are 2003 Tropical Atmosphere Ocean (TAO) on the NOAA R/V

91   *Ronald H. Brown*, 2004 Biocomplexity (hereinafter BIO) on the R/V *Steward Johnson*,

92   2007 Deep Ocean Gas Exchange Experiment (DOGEE) on the UK ship RRS *Discovery*,

93   2008 Southern Ocean Gas Exchange Experiment (SO GasEx) on *Ronald H. Brown*, and

94   2008 Vamos Ocean-Cloud-Atmosphere-Land Study Regional Experiment (VOCALS-

95   REx, hereinafter VOCALS) on *Ronald H. Brown*. The location, time, DMS sea-to-air

96   flux, seawater DMS concentration, and reference for each cruise are listed in Table 1.

97   While the environmental conditions of each cruise individually were not highly

98   variable, together these five cruises encompass a large range in wind speed (1 ~ 21 m s^{-1}),

99   sea surface temperature (SST, 2~30°C), and atmospheric boundary layer stability

100   (statically unstable to stable), which is shown in Fig. 2. The higher winds, lower SST,

101   and frequent occurrences of stable boundary layer set SO GasEx apart from other cruises.

102   A compilation of k_{DMS} from these projects allows us to assess our current understanding

103   of gas exchange in an effort to improve existing models.

104

105   **2. Experimental**

106   *2.1 Background on SO GasEx*

107   The Southern Ocean is characterized by sustained periods of high winds, low

108   SST, and large seasonal cycles in biological productivity. Gas exchange between the

109   ocean and atmosphere in the Southern Ocean plays an important role in the global climate

110   through, for example, the sequestration of atmospheric CO_2 via production of polar

111   bottom waters and through the role of DMS emissions in generation of atmospheric

112   sulfate aerosols. The Southern Ocean GasEx experiment was conceived as the third in a

113   series of projects combining direct measurements of gas exchange with concurrent

114   studies of related biological and physical processes, focused on the unique high wind

115   conditions of the Southern Ocean. SO GasEx included a ^{3}He/SF_6 tracer patch study [*Ho*

116   *et al.*, this issue b], and EC observations of CO_2 [*Edson et al.*, this issue] as well as DMS

117   (this paper). The eddy covariance measurement of DMS flux using the atmospheric

118   pressure ionization mass spectrometer (APIMS), including error analysis, is detailed

119   recently by [*Blomquist et al.*, 2010] and will not be described further here.

120

121   *2.2 Measurements of Seawater DMS Concentration*

122   Seawater DMS (DMS_w) concentration near the surface was measured by a gas

123   chromatograph. For SO GasEx, DMS_w was measured at ~7 minute intervals using a

124   semi-continuous analytical system linked to an equilibration device. Seawater from the

125   ship's clean water supply at ~5 m depth was passed through a membrane equilibrator

126   (Liqui-Cel®, Extra-Flow 2.5 x 8) at ~400 mL min^{-1}. Nitrogen was passed through the

127   equilibrator at a continuously monitored flow rate of 40 mL min^{-1} and pressure of 150

128   kPa. DMS was trapped on an adsorbent (Carbopack-X, Sigma-Aldrich®) at -50 ºC and

129   measured on a Varian 3800 gas chromatograph equipped with a pulsed flame photometric

130   detector (PFPD). The system was calibrated and sensitivity monitored hourly using a

131   permeation device (Dynacal®, Vici Metronics Inc.) delivering 120 ng DMS min^{-1} at 30

132   °C. In DOGEE, DMS_w was sampled every 7~10 min from a towed Fish at 1~2 m below

133   the surface and quantified using a purge-and-cryogenic trap linked to a Varian 3800 gas

134   chromatograph with PFPD. A similar purge-and-trap method was used on the TAO and

135   VOCALS projects, but at a lower frequency of every 15~30 minutes [*Bates et al.*, 2000].

136   The BIO cruise was a Lagrangian water mass study following a cyclonic and an

137   anticyclonic eddy. DMS_w was determined from the shallowest bin (~5 m) of CTD casts

138   [*Kiene and Service*, 1991] and showed little variation as a result of the Lagrangian

139   design. Limited inter-comparisons between manually collected surface samples and the

140   ship's seawater sampling system during DOGEE and SO GasEx suggest that there was

141   no significant, systematic gradient in DMS_w in the top 5 m of the water column in

142   moderate winds. Nor was there a discernible difference in concentration caused by the

143   different means of water sampling.

144

145   *2.3 Diffusivity Normalization on the Transfer Velocity*

146   The diffusivity dependence of gas transfer can be described by the Schmidt

147   number (S_c) as the ratio between kinematic viscosity (v) of seawater and molecular

148   diffusivity (D), both functions of temperature and (to a lesser degree) salinity [*Saltzman*

149   *et al.*, 1993]. To remove variance due to diffusivity, it is common to normalize transfer

150   velocity measured at ambient conditions to a reference S_c of 660:

151   $k_{660} = k_{DMS}(660/S_c)^n$ (3)

152   The exponent n is thought to vary from -2/3 for a rigid surface to -1/2 for a rough surface;

153   we assume the latter for the open ocean. A Schmidt number of 660 corresponds to 20 C°

154   for CO_2 in seawater and 27.2 C° for DMS. A relationship similar to (3) is also frequently

155 used to account for diffusivity differences among gases, as in the derivation of k_{660} for a

156 specific gas of interest from k_{660} of ^{3}He/SF$_6$ obtained from deliberate tracer studies. The

157 analysis below suggests this may lead to substantial bias at moderate to high wind speeds

158 when the solubility of the gas of interest differs significantly from that of the tracer gas.

159   Figure 3 shows time series of atmospheric and seawater DMS concentrations,

160 DMS flux, 10-m wind speed, transfer velocity at ambient condition and normalized to S_c

161 of 660, as well as the DMS Schmidt number from SO GasEx. Elevated DMS flux clearly

162 corresponded to higher DMS$_w$ at times, such as on March 14 and 24, but not always

163 because of variable winds. Towards the end of the experiment, the ship encountered a

164 storm while in transit to Uruguay. Wind speed briefly exceeded 20 m s^{-1} and the surface

165 water was much warmer (~14 °C) during this period than what was typical of SO GasEx

166 (~5 °C). However, DMS flux and transfer velocity were not elevated, while DMS$_w$ was

167 similar to earlier periods of the project.

168

169 **3. Data Refinement**

170 *3.1 Basic Data Filtering*

171   Uncertainty in k_{660} hinges principally on the precision and sampling variability of

172 the flux and DMS$_w$. There is substantial noise in EC flux observations that is independent

173 of the measurement system. This scatter originates from sampling a stochastic process

174 (turbulence) over relatively short time scales where low frequency contributions to flux

175 are poorly sampled. Even for a well-resolved scalar like water vapor, the sampling

176 uncertainty of an hourly flux is on the order of 25% [*Fairall et al.*, 2003]. At a wind

177 speed of ~8 m s^{-1} and in a near-neutral boundary layer, *Blomquist et al.* [2010] showed

178   that relative uncertainty in hourly DMS flux is on the order of ~30%. Uncertainty further

179   increases when the boundary layer is stable, which is discussed in the next section. For a

180   large number of hourly observations, however, precision in the mean flux estimate

181   improves significantly. Here, we focus on screening out conditions that might lead to

182   nonrandom biases in the measured flux.

183   From the lag correlation calculation between DMS_a and vertical wind velocity

184   (w), we find a clear peak in correlation and a corresponding lag time of ~1.5 seconds

185   (depending on the inlet length and flow rate) when the wind is from the bow sector.

186   When the wind is coming from the stern quadrant, however, DMS_a and w show poor

187   correlation due to severe airflow distortion by the ship's superstructure. For SO GasEx,

188   three sonic anemometers were mounted on the foremast of the *Ronald H. Brown* at 18 m,

189   with one in the middle and two others ~1 m to the port and starboard sides. The DMS

190   sampling inlet was located near the base of the middle anemometer. We limit relative

191   wind direction to ±60° from the bow for the middle anemometer and -120° to 0° and 0°

192   to 120° for the port and starboard anemometers, respectively. DMS fluxes are computed

193   at 10-minute intervals from all three anemometers and averaged when two or more

194   anemometers are in-sector. On all other cruises with a single anemometer, a limit in

195   relative wind direction of ±60° from the bow is applied. Similar airflow distortions can

196   occur when the ship is turning rapidly. Thus 10-minute flux segments when the range in

197   gyro heading exceeds 10 degrees are eliminated. Hourly averages are computed from the

198   valid 10-minute results.

199   In Fig. 4, hourly k_{660} satisfying the above criteria from all five cruises are plotted

200   vs. U_{10}, including the brief high wind speed period (>20 m s^{-1}) from SO GasEx. During

9

201   this storm encounter, the sea was characterized by fully developed long swells and the

202   measured k_{DMS} was much lower than the trend extrapolated from intermediate winds. To

203   date, we have not identified a measurement error responsible for the low k_{DMS}. There

204   may be an environmental factor involved, but pending a more detailed analysis of this

205   event, we will not consider these points further in this section.

206   To more clearly examine the trend in k_{660} as a function of wind speed, we plot k_{660}

207   from the five cruises averaged to U_{10} bins in Fig. 5. While overall k_{660} increases with

208   U_{10}, k_{660} from tropical cruises such as TAO appears to be higher than that from the high

209   latitude SO GasEx, particularly in high winds. A similar SST trend is observed by

210   *Marandino et al.* [2009] in their synthesis of k_{DMS} measurements. Also included in Fig. 5

211   is the k_{DMS} curve computed from the NOAA COARE gas transfer model (discussed in

212   detail below) using parameters A=1.3 and B=1.0 at 27.2 °C.

213   Another source of uncertainty in k_{660} is variability in discretely sampled DMS_w.

214   When DMS_w shows high temporal or spatial variability, uncertainty in the hourly mean

215   waterside concentration increases; the location of DMS_w measurement is also less likely

216   to correspond to the flux footprint. For a measurement height of 18 m and a wind speed

217   of 8 m s^{-1}, the flux footprint covers a region several hundred meters upwind of the ship

218   under neutral or unstable conditions; the footprint can be much larger under stable

219   conditions [*Horst and Wiell*, 1994]. We address the variability in DMS_w by setting a

220   threshold of 0.25 for the relative standard error of the mean in the hourly DMS_w for all

221   cruises except BIO, following *Huebert et al.* [2010].

222

223   *3.2 Effect of Atmospheric Stability*

224   The wind speed profile as a function of height depends on boundary layer

225   stability. At a reference height of 10 meters, wind speed is related to wind stress through

226   u_* and the 10-m drag coefficient (C_{D10}): $u_* = C_{D10}^{1/2}U_{10}$. Adjusted to neutral condition,

227   the relationship becomes $u_* = C_{D10n}^{1/2}U_{10n}$, where C_{D10n} and U_{10n} are stability-corrected.

228   Logic follows that some of the variability in the k vs. U_{10} relationship is due to the effect

229   of stability on the logarithmic wind speed profile. We estimate u_*, U_{10n}, z_0 (roughness

230   length), and L (Monin-Obukhov length scale) from bulk meteorological variables using

231   the NOAA COARE 3.0 bulk flux model [*Fairall et al*., 2003]. The covariance wind

232   stress measurements are not used here because of the associated sampling challenges on a

233   moving platform, especially in high wind environments such as SO GasEx. Measuring

234   covariance flux of a scalar (e.g. DMS) requires motion-corrected vertical wind velocity

235   (W) only, whereas measuring momentum flux is more difficult because the measurement

236   can be contaminated if there remains artifact crosstalk between motion-corrected W and

237   U.

238   The stability of the atmospheric boundary layer can be represented by the ratio

239   z/L, with z being the sensor height. The ratio z/L depends on the air-sea temperature

240   difference, and is a proxy for the relative contribution to turbulence generated by

241   buoyancy and shear. A significantly positive z/L indicates a statically stable boundary

242   layer, usually caused by warm air over cold water. A negative z/L is statically unstable,

243   and $z/L \approx 0$ implies a near neutral condition. Figure 6 shows DMS k_{660} vs. U_{10} and U_{10n}

244   for SO GasEx. The degree of scatter in k_{660} is reduced when U_{10n} is used, with the

245   difference most noticeable in low-to-moderate winds where buoyancy-driven convection

246   is more important. The coefficient of determination (r^2) for a linear relationship between

11

247   k_{660} and wind speed is improved from 0.51 to 0.56 with U_{10n} instead of U_{10}.

248   Besides modifying the wind speed profile, stability in the boundary layer

249 increases uncertainty in the flux measurement [*Blomquist et al.*, 2010]. Stable conditions

250 lead to suppression of turbulent eddies and possibly a shallow boundary layer. While

251 damping of turbulence may be less significant in moderate to high winds due to the high

252 surface shear, strong, warm winds over a cooler ocean surface are often found in warm

253 sectors of frontal passages. While damping of turbulence in these conditions may not be

254 very significant due to the high surface shear, the boundary layer can become quite

255 shallow. With all else being constant, a shallower boundary layer implies a steeper flux

256 gradient, which results in a greater systematic underestimate of the true surface flux, as

257 illustrated in Fig. 6 by the solid circles ($z/L > 0.05$). The r^2 between k_{660} and U_{10n} is also

258 lower (0.30) for these hours of more stable conditions. We hereafter omit hourly flux

259 observations when $z/L > 0.05$. This stability threshold is intended to remove conditions

260 unfavorable for EC measurement and does not imply a cessation of turbulence. This

261 filter removes about 30% of our observations from high latitude cruises (SO GasEx and

262 DOGEE), while data from the tropical and temperate waters are basically unaffected.

263 About 1100 hourly k_{DMS} observations from all cruises remain following screening for

264 DMS_w and stability.

265

266 *3.3 Flux Corrections at High and Low Frequencies*

267   Some flux signal is lost at the lowest frequencies in 10-minute time intervals, and

268 of the lowest frequencies that are measured, the sampling statistics are poor. Additional

269 flux signal is lost at the highest frequencies due to an attenuation of small-scale

270   fluctuations by the inlet system and the Nafion® air drier, which is needed to remove

271   water from the ambient air and increase the sensitivity of the APIMS towards DMS. We

272   partially correct hourly cospectra for high frequency inlet-attenuation based on an

273   empirical frequency response function (a correction of a few percent, *Blomquist et al.*,

274   [2010]). An estimate for additional losses is then obtained through comparison with a

275   theoretical cospectral function for neutral conditions [*Kaimal et al.*, 1972]. Partially

276   corrected cospectra are normalized to DMS_w and $S_c = 660$ and bin-averaged by relative

277   wind speed (U_R). For each U_R bin, the theoretical Kaimal function is fit to the observed

278   data over a restricted frequency range (0.008~1 Hz). Measurement height and relative

279   wind speed parameters in the fit are fixed to mean observed conditions. Within each bin,

280   the difference in area under the high and low frequency tails (0~0.005 Hz and 1~10 Hz)

281   between the fit and the observed cospectrum is taken as an estimate of the missing flux.

282   A cospectral correction factor (F_C) is computed as the ratio between the total corrected

283   flux and the observed flux for each bin and fit to a polynomial as a function of U_R:

284    $F_c = 1.165 - 0.020U_R + 0.001U_R{}^2$ for SO GasEx. The estimated correction to the flux is

285   less than 10% across the range of wind speeds for SO GasEx and less than 5% in

286   moderate winds. The magnitude of the correction varies somewhat among cruises

287   because of variable sampling height, inlet length, flow rates, etc.

288

289   *3.4 Airside Resistance*

290   Airside resistance to exchange of sparingly soluble tracer gases is small and

291   usually neglected. However, as the solubility (α) of a gas increases with decreasing

292   temperature, the airside resistance becomes more important. Rearranging (2), *McGillis et*

293 *al*. [2000] defined the atmospheric gradient fraction γ_a as the fraction airside contribution

294 to total concentration difference: $\gamma_a = [1 + k_a(\alpha k_w)^{-1}]^{-1}$. For DMS, γ_a is on the order of

295 0.05 at 20 °C, compared to only ~0.002 for the less soluble CO_2. Thus, the temperature

296 dependence in airside resistance, which is not accounted for in (3), is more significant for

297 DMS than for CO_2. k_{DMS} obtained from (1) represents the total transfer velocity. To

298 account for all temperature effects when normalizing to $S_c = 660$, the airside and

299 waterside transfer velocity need to be specified and adjusted separately. Following

300 *McGillis et al*. [2000], we estimate k_a of DMS as $659 U_{10n}(MW_{DMS}/MW_{H_2O})^{-1/2}$ [cm hr^{-1}],

301 with *MW* representing molecular weight. To approximate k_w a priori, we use the

302 formulation from the NOAA COARE gas transfer model [cm hr^{-1}]:

303 $$k_w = 360000 u_*(\rho_w/\rho_a)^{-1/2}[h_w S_c^{1/2} + \kappa^{-1}\ln(0.5/\delta_w)]^{-1} + B(2450 f_{wh} G) \qquad (4)$$

304 Here ρ_w is the density of water, δ_w the waterside molecular sublayer thickness, κ the von

305 Karman's constant (0.4), and $h_w = 13.3/(A\phi)$. In h_w, A is an empirical constant and tuned

306 to 1.3 by *Blomquist et al*. [2006] using tropical EC measurements of DMS; φ accounts for

307 surface buoyancy flux enhancement of the transfer and only becomes important in wind

308 speed less than ~2 m s^{-1}. The second term on the RHS of (4) is the parameterization of k_b

309 from *Woolf* [1997], where the whitecap fraction $f_{wh} = 3.84$ x 10^{-6} $U_{10}^{3.41}$ [*Monahan and*

310 *O'Muircheartaigh*, 1980], and $G = \alpha^{-1}[1 + (14\alpha S_c^{-1/2})^{-1/1.2}]^{-1.2}$. B is an empirical constant,

311 to which we assign the provisional value of 1.0 [*Blomquist et al*., 2006].

312   At typical SO GasEx temperatures (~5 °C), γ_a for DMS is about 0.10 at a wind

313 speed of 15 m s^{-1}. The airside effect calculated here is smaller than was estimated by

314 *McGillis et al*. [2000] for DMS because they used the parameterization from *Wanninkhof*

315 [1992] for k_w, which significantly overestimates k_{DMS} at high wind speeds. We can now

316   estimate the ambient waterside transfer velocity of DMS from measured k_{DMS}:

317    $k_w = k_{DMS}/(1-\gamma_a)$. Applying the Schmidt number normalization to k_w yields k_{w660}. For

318   consistency, the airside transfer should also be adjusted to 27.2 °C ($S_c = 660$ for DMS),

319   such that the total normalized transfer velocity becomes:

320    $$k_{660} = [\frac{1}{k_{w660}} + \frac{\alpha_{660}}{k_a}]^{-1}$$ (5)

321   Here α_{660} represents the solubility of DMS at 27.2 °C (10.4). Compared to the S_c-only

322   normalization specified by (3), separate treatment of the temperature dependence in

323   waterside and airside transfer given by (5) increases k_{660} from SO GasEx by ~4%.

324   After screening for DMS_w variability as well as atmospheric stability, and

325   accounting for temperature dependence in airside resistance, r^2 for a linear relationship

326   between k_{660} from (5) and U_{10n} for all cruises is increased from 0.63 in Fig. 4 to 0.71 in

327   Fig. 7. However, discrepancies in k_{660} remain among different cruises, particularly in

328   higher winds, which might be in part related to the temperature dependence in bubble-

329   mediated transfer.

330

331   **4. Bubble-mediated Exchange and Solubility Normalization**

332   When waves break, air is trapped in water and entrained to depth of a few meters

333   in the form of bubbles, which then rise and exchange gas with the surrounding water.

334   The amount of a trace gas partitioning into air bubbles from the bulk water likely depends

335   on both solubility and diffusivity. At lower temperatures, α increases and less gas is

336   transferred from the bulk water to bubbles. The bubble component of k_{DMS} should be

337   normalized to a reference temperature separately from the interfacial component, which

338   does not depend on α. It is convenient to first estimate the interfacial component of gas

15

339   exchange due to shear (k_v), ignoring buoyancy-driven exchange that is insignificant in

340   moderate-to-high winds. An estimate for bubble-mediated transfer velocity (k_b) is then

341   simply the difference between k_w and k_v:

342    $$k_b = k_w - k_v = k_w - k_{v660}(660/S_c)^{1/2} = (k_{w660} - k_{v660})(660/S_c)^{1/2} \qquad (6)$$

343   Here k_{v660} is interfacial transfer velocity normalized to $S_c = 660$. We estimate k_{v660} as a

344   linear function of the tangential component of the friction velocity (u_{*v}) due to viscous

345   wind shear (i.e. $k_{v660} = C_1 + C_2 u_{*v}$, as described below). To account for the solubility

346   effect in k_b, we normalize it to a reference temperature of 27.2 C° ($S_c = 660$ for DMS)

347   using the S_c and α dependence (G) described by the *Woolf* [1997] model for bubble-

348   mediated exchange. Adding the interfacial component yields the solubility and diffusivity

349   normalized waterside transfer velocity: $k_{w660}' = k_{v660} + k_b(G_{660}/G)$, where G_{660} is the

350   Schmidt number-solubility dependence at 27.2 °C. We may then substitute k_{w660}' in

351   place of k_{w660} in (5) to yield the final normalized total transfer velocity (k_{660}'). While the

352   procedure described above is simple, the justification and background require more

353   detailed explanations, which will be covered in the remainder of this section.

354

355   *4.1 Quantifying the Interfacial Transfer Velocity*

356   From the two-layer model described by *Liss and Slater* [1974], physical processes

357   that thin the diffusive sub-layers are conceptualized to enhance direct (interfacial) gas

358   exchange through a reduction in resistance. Shear (viscous) stress from wind blowing

359   tangentially to the sea surface is usually the most important of such processes, as it leads

360   to micro-scale breaking of capillary waves and wavelets that are largely responsible for

361   interfacial gas exchange [*Frew et al.*, 2004]. Surface renewal models from *Csanady*

16

362 [1990] and *Soloviev and Schlüssel* [1994] predict that without bubbles, *k* should be

363 linearly related to u_*, consistent with our k_{DMS} observations from DOGEE in moderate

364 winds [*Huebert et al.*, 2010].

365 In high winds and mature seas, the surface ocean transitions from micro-scale

366 breaking to the breaking of long gravity waves. As total surface stress grows with wind

367 speed, an increasingly larger fraction is partitioned to wave stress, which includes

368 momentum transfer into the ocean by breaking waves and form drag. While wave

369 breaking can lead to more gas exchange via enhanced turbulence and bubble plume

370 formation, increasing partition of total stress to form drag, which is a result of the

371 pressure differential developed between the front and lee sides of large waves, may

372 suppress micro-scale breaking [*Banner et al.*, 1989] and potentially reduce the wind

373 speed dependence of *k*. The net effect of these competing mechanisms on *k* in high

374 winds partly depends on gas solubility. Since wave stress does not significantly

375 contribute to thinning of the diffusive sub-layer, a linear relationship between k_ν and $u_{*\nu}$

376 should be more general than that between *k* and u_* and hold true even in high winds,

377 concurrent with the additional decrease in transfer resistance due to bubbles and

378 whitecaps.

379 We determine $u_{*\nu}$ from the tangential component of wind stress. The COARE

380 bulk flux algorithm follows *Smith* [1988] and partitions total roughness length as:

381 $z_o = \varphi u_*^2 / g + 0.11 \nu / u_*$ (7)

382 where φ is a fit to drag coefficient observations and *g* is gravity. The first term on the

383 right hand side of (7) is due to waves, and the second due to smooth flow. From

384 laboratory wind-wave studies, *Banner and Peirson* [1998] found that total stress in the

385   smooth flow regime represents the upper limit for the tangential stress. Based on this

386   result, *Mueller and Veron* [2009] (hereinafter MV09) estimate the 10-m tangential drag

387   coefficient in neutral condition (C_{D10v}) as a function of the smooth flow roughness length:

388    $C_{D10v}{}^{1/2} = \kappa/\log(10/(0.11\nu/u_{*v}))$ (8)

389   Here κ is the von Karman's constant ($\approx$0.4). Thus at a given wind speed, u_{*v} can be

390   computed iteratively: $u_{*v} = C_{D10v}{}^{1/2}U_{10n}$. The result of this partition of the total wind

391   stress to the tangential and wave component is qualitatively similar to the alternate

392   estimate by *Soloviev and Schlüssel* [1996] (hereinafter SS96), as shown in Fig. 8. SS96

393   use the Keulegan number defined by *Csanady* [1978] as the criterion for the transition to

394   large-scale wave breaking: $Ke = u_{*w}{}^3/(g\nu)$, where u_{*w} is the waterside transfer velocity.

395   Tangential stress is estimated as a fraction of total stress: $(1 + Ke/Ke_{cr})^{-1}$. Ke_{cr} is the

396   critical Ke, an empirically derived threshold dependent on wave age and speculatively set

397   to 0.45 here for illustration. Tangential stress from SS96 varies with wave age, whereas

398   u_{*v} from MV09 does not (only the wave component does). We adopt the MV09's

399   approach because Ke is not required, as tangential stress is independent of the

400   specification of total drag coefficient (i.e. u_* is not required to estimate u_{*v}).

401   Because of the increasing importance of wave stress with wind speed, C_{D10v}

402   decreases in high winds and u_{*v} shows a slight downward curvature, with estimates from

403   SS96 rolling off more. If k_v follows u_{*v} in high winds, it too should roll off slightly. We

404   don't expect this to significantly affect the total transfer of a relatively insoluble gas (e.g.

405   CO_2) in high winds because the additional bubble-mediated exchange term overwhelms

406   any suppression in interfacial exchange. However, for a soluble gas like DMS with a

407   more modest bubble enhancement, the difference between k_v and k should be smaller.

408   Indeed, if we plot k_{660} vs. u_* for our DMS observations, the curve would be best

409   described as linear in moderate winds with a slight leveling off in high winds,

410   qualitatively similar to the "wave attenuation" effect observed for DMS in the laboratory

411   by *Rhee et al*. [2007]. This roll off suggests that the behavior of k_{DMS} in high winds is

412   related to reduced partition of total stress to the tangential component.

413   Let us now examine how k_{w660} relates to u_{*v} in different wind speed regimes for

414   all cruises (Fig. 9). In the calmest conditions ($u_{*v} < {\sim}0.1$ m s^{-1}, corresponding to a wind

415   speed of 2~3 m s^{-1}), the slope between k_{660} and u_{*v} appears to be relatively flat, likely

416   because buoyancy-driven convection is more important than wind shear at driving gas

417   exchange. The slope steepens with increasing wind speeds; a linear fit from 2~6 m s^{-1}

418   yields an intercept (C_1) of -3.8 and a slope (C_2) of 69.7. We interpret the extrapolation of

419   this fit to higher winds as interfacial transfer velocity (k_{v660}), which becomes less than the

420   bin-average k_{w660} above $u_{*v} \approx 0.2$ m s^{-1} (a wind speed of 7~8 m s^{-1}, or the onset of

421   whitecap formation). Subtracting k_{v660} from k_{w660} in moderate-to-high winds and

422   removing the prior S_c normalization yield an estimate of k_b, which is relatively small for

423   DMS.

424

425   *4.2 Solubility Normalization of Bubble-mediated Exchange*

426   Normalizing k_b to a reference temperature requires a model describing the S_c and

427   α dependence in bubbles. Scaling up from a single bubble model, *Woolf* [1997]

428   parameterizes k_b of CO_2 to be proportional to whitecap fraction (f_{wh}) and G. A linear

429   relationship between k_b and f_{wh} was proposed by *Monahan and Spillane* [1984] and

430   confirmed by laboratory results of *Asher et al*. [1996] with optically measured bubble

431   plume coverage as the analog for f_{wh}. The term $G = \alpha^{-1}[1 + (14\alpha S_c^{-1/2})^{-1/1.2}]^{-1.2}$ contains

432   the solubility and diffusivity dependence in k_b. *Woolf* [1997] identifies the two

433   asymptotic behaviors of bubble-mediated exchange at opposing limits of gas solubility.

434   For an insoluble gas with a very small α, G approximately scales as $S_c^{-1/2}$. This implies

435   the temperature dependence in solubility has little effect on k_b for gases like SF_6 and the

436   usual normalization to $S_c = 660$ accounts sufficiently for temperature dependencies. For

437   a more soluble gas (large $\alpha\square$), G approaches α^{-1} and the S_c dependence vanishes. For

438   DMS at 5 C° (the approximate mean SST during SO GasEx), $\alpha = 28.3$ and $S_c = 2050$; the

439   functional form of G is close to α^{-1}, with a weak S_c dependence. Multiplying k_b by the

440   factor (G_{660}/G) yields the normalized bubble-mediated transfer velocity, which is then

441   summed with the prior estimate of k_{v660} to yield the final normalized waterside transfer

442   velocity (k_{w660}'). For SO GasEx, the normalization to 27.2 °C increases k_b by ~150%, or

443   ~40% relative to k_b adjusted using the S_c-only dependence. Together with interfacial

444   exchange, k_{w660}' is ~6% greater than k_{w660} in high winds. While the effect of this

445   normalization appears to be small and only secondary in importance, for a larger k_b (e.g.

446   if k_v rolls off more in high winds, as in SS96), the adjustment in k_b would be

447   correspondingly greater as well.

448   *Keeling* [1993] and *Asher et al.* [1996] describe somewhat different dependences

449   on S_c and α in bubble-mediated exchange than *Woolf* [1997]. *Keeling* [1993] models k_b

450   based on bubble spectra photographically recorded in laboratory experiments designed to

451   simulate wave breaking [*Monahan and Zeitlow*, 1969; *Cipriano and Blanchard*, 1981],

452   with a range in bubble radius from ~0.03 mm to 4 mm. The author suggests that

453   relatively large bubbles (>0.5 mm in radius) contribute significantly to k_b, which should

454   scale roughly as $\alpha^{-0.3} S_c^{-0.35}$. *Asher et al*. [1996] measured the exchange of multiple gases

455   in a tipping-bucket whitecap simulation tank. Following *Memery and Merlivat* [1985],

456   *Asher et al*. [1996] separate k_b to contributions from bubbles that dissolve in or

457   equilibrate with the surrounding water before reaching the surface and ones that never

458   equilibrate: $k_b = a\,\alpha^{-1} + b\,\alpha^{-0.37} S_c^{-0.18}$. Theoretically, small bubbles with long lifetimes

459   tend to be dissolved or equilibrated; k_b due to these bubbles should scale as α^{-1} (not

460   limited by diffusivity). On the other hand, large bubbles that rise rapidly have

461   insufficient time to equilibrate with the bulk water before surfacing. Gas is exchanged

462   between the bulk water and these large bubbles during their entire lifetime, implying that

463   k_b depends on both α and S_c. For evasion and through a cleaned surface, *Asher et al*.

464   [1996] estimate that gas exchange due to dissolving and equilibrating bubbles is orders of

465   magnitude smaller than that due to non-equilibrating bubbles ($a = -1 \times 10^{-4}$ and $b = 1.7 \times$

466   10^{-2}, in units of m s^{-1}), implying that the overall functionality of k_b for evasion is

467   approximately $\alpha^{-0.37} S_c^{-0.18}$. If we assume a weaker solubility dependence in k_b, as

468   suggested by *Keeling* [1993] and *Asher* et al. [1996], the temperature effect in k_b will be

469   correspondingly smaller than what we have shown. Over the SST range of 5~27 °C, the

470   formulation $\alpha^{-0.37} S_c^{-0.18}$ for DMS differs by a factor of ~1.8, whereas the *Woolf* [1997]

471   formulation differs by a factor of ~2.5. Coincidentally, $S_c^{-0.5}$ for DMS over the same SST

472   range also differs by a factor of ~1.8. Thus, using the formulation from *Asher et al*.

473   [1996] to adjust k_b leads to the essentially the same result as using the widely used S_c-

474   only normalization.

475   The error caused by ignoring the temperature dependence in solubility when

476   normalizing transfer velocity to $S_c = 660$ is the most significant for gases of intermediate

477   solubility. Using the COARE model, we can calculate the difference between k_b (G_{660}/G)

478   and k_b $(660/S_c)^{-1/2}$ for a normalization from 5 C° to the temperature at which $S_c = 660$ for

479   a range of gases, and compute the relative error by dividing that difference by k_{660}. This

480   is shown in Fig. 10 for DMS, CO_2, methyl iodide (CH_3I), and chloroiodomethane

481   (CH_2ClI). In seawater, $S_c = 660$ at 24.0 and 27.8 C° for CH_3I, and CH_2ClI; the respective

482   α values are 3.6 and 18.8 [*Archer et al.*, 2007]. It is apparent that for very insoluble

483   gases, the relative error in transfer velocity in high winds is near zero because the

484   temperature dependence of G is similar to $S_c^{-1/2}$, meaning that the standard S_c

485   normalization is adequate. Such is the case for CO_2, as well as SF_6, radon, and nitrous

486   oxide (not shown). For soluble gases, the temperature dependence of G diverges more

487   from $S_c^{-1/2}$, but the magnitude of k_b also decreases, so the error in total transfer velocity is

488   also low. It is transfer of gases with intermediate solubility, such as organosulfur

489   compounds, that are affected the most by the temperature dependence in solubility.

490   Normalizing DMS and CH_3I from 5 C° to the reference S_c only will lead to

491   underestimations in k_{660} of ~7 and 11%, respectively at a wind speed of 16 m s^{-1}.

492

493   **5. Discussion**

494   Replacing k_{w660} in (5) with the k_{w660}' yields the final normalized total transfer

495   velocity (k_{660}'), which is plotted in U_{10n} bins for all five cruises in Fig. 11. Compared to

496   Fig. 5, k_{660}' is greater than k_{660} from (3) for the coldwater SO GasEx by ~7 cm hr^{-1} at 15

497   m s^{-1}, whereas for the tropical TAO and BIO cruises, k_{660}' is slightly lower than k_{660} at

498   most wind speeds. To more clearly demonstrate the effects of filtering for DMS_w

499   variability and atmospheric stability, normalizing for temperature dependence in airside

22

500   resistance, and adjusting for both α and S_c dependence in k_b, Fig. 12(a) shows the

501   difference between k_{660} from (3) and COARE model estimate at 27.2 °C in U_{10} bins; (b)

502   shows the difference between final normalized k_{660}' and COARE estimate in U_{10n} bins. The

503   COARE gas transfer model estimate is used as a reference here for comparison. The

504   divergence at high wind speeds shown in Fig. 12(a) illustrates the biases among cruises

505   partly due to the residual temperature dependence not accounted for by (3). k_{660}' from all

506   cruises show closer agreement with each other; at 9 m s^{-1}, the standard deviation of the

507   bin-averages is 3.6 cm hr^{-1} for k_{660} and is reduced to 2.3 cm hr^{-1} for k_{660}'. Table 2

508   contains the bin-average k_{660} (from (5), accounting for temperature-solubility dependence

509   in airside resistance, but not in bubbles) and k_{660}' of the five cruises, weighted by the

510   number of points per bin for each cruise. Average k_{DMS} from SO GasEx at ambient

511   conditions and corresponding u_* values in U_{10n} bins from 1 to 15 m s^{-1} are also presented.

512   We can now compare this average k_{660}' to previous observations of relatively

513   insoluble gases and widely used wind speed-dependent parameterizations (Fig. 13).

514   Based on measurements of SF_6 gas exchange in a lake and wind tunnel observations, *Liss*

515   *and Merlivat* [1986] model *k* as three piece-wise linear functions of wind speed with

516   increasing slope at higher winds, representing distinctive regimes of smooth surface,

517   rough surface (capillary waves), and breaking waves, respectively. From natural [14]C

518   disequilibrium and the bomb ^{14}C inventory, *Wanninkhof* [1992] derive *k* as a quadratic

519   function of wind speed. From artificial injections of two volatile tracers ([3]He and SF_6)

520   and one non-volatile tracer (spores) in the North Sea, *Nightingale et al.* [2000] report a

521   parameterization of *k* that consists of both linear and quadratic dependences on wind

522   speed. *Ho et al.* [2006] fit a quadratic function to [3]He/SF_6 measurements in the Southern

523 Ocean. Based on EC observations of CO_2 during the GasEx I cruise in the North Atlantic

524 (a CO_2 sink), *Wanninkohf and McGillis* [1999] suggested a cubic fit between k and wind

525 speed. However, an equivalent study during the follow-up GasEx II cruise in the

526 Equatorial Pacific (a CO_2 source) resulted in a much weaker wind speed dependence

527 [*McGillis et al.* 2004]. The authors attributed the GasEx II result to a limited wind speed

528 range and strong diurnal heating.

529   Also shown in Fig. 13 are the k_{660} curves from the COARE gas transfer model for

530 DMS (A=1.3; B=1.0; SST=27.2 °C) and CO_2 (A=1.3; B=1.0; SST=20.0 °C). Normalized

531 for diffusivity, k_{660} of different relatively insoluble gases due to buoyancy and shear is

532 expected to be similar [*Asher et al.*, 1996]. Indeed, below 7~8 m s^{-1}, before the onset of

533 whitecapping, k_{660} of the different gases are comparable. The lone exception is GasEx II,

534 which shows a much higher k_{660} in low winds. In higher winds, transfer velocity of DMS

535 is significantly lower than that determined for CO_2 and from ^{3}He/SF$_6$ due to the much

536 higher solubility of DMS, and hence decreased partitioning into air bubbles. While a

537 power law parameterization of k as a function of wind speed might be adequate in

538 application for one particular gas, it masks the complex physical mechanisms responsible

539 for gas exchange in high winds and rough seas. To more accurately quantify the

540 interfacial and bubble-mediated components of air-sea exchange, simultaneous high wind

541 speed measurements of the transfer velocity of multiple gases with a large range of

542 solubility will be needed.

543   In general, the COARE gas transfer model appears to predict DMS transfer

544 velocity fairly well at the reference S_c. A better assessment of model performance is a

545 comparison between the observed k_{DMS} and modeled k_{DMS} at ambient conditions, as

546   normalization to a reference will introduce additional uncertainty due to assumptions in

547   S_c and α. Such uncertainty amplifies when the SST is very different from 27.2 °C, as was

548   the case for SO GasEx. Since SST is a required input parameter for COARE 3.0 and the

549   gas transfer parameterization for k_b accounts for solubility and diffusivity effects, no

550   adjustment on the model output is necessary for a direct comparison of k_{DMS}.

551   Figure 14 shows the residual difference (observation minus model) in k_{DMS} for all

552   five cruises, which on average is within 2 cm hr^{-1} across the wind speed range. In low

553   winds, our DMS observation appears to be less than the COARE prediction, which may

554   result from measurement errors or model deficiencies. Relative uncertainty in the EC

555   flux observations increases in low winds as a result of the lower signal to noise ratio and

556   a shift of turbulent eddies towards lower frequencies that are less adequately captured by

557   our averaging intervals. Near surface gradients in DMS_w are also more likely in calm

558   conditions, which would lead to bias in the measured DMS_w sampled at a few m below

559   the surface. With regard to the model, COARE uses the oceanic turbulent Richardson

560   number and heat fluxes to determine the buoyancy contribution to gas exchange.

561   Uncertainty in the critical turbulent Richardson number, an empirical constant that

562   defines the threshold from free convection to forced convection, is an additional source of

563   error. Overall, this discrepancy does not greatly bias the predicted global mean flux

564   because of the small magnitude of k_{DMS} in calm conditions.

565   In moderate winds, observations and COARE prediction agree closely, implying

566   that the empirical parameter $A = 1.3$ for direct transfer is reasonable (the bin-average at 9

567   m s^{-1} shows a small positive bias partly due to the several high k_{DMS} points between 8~9

568   m s^{-1}). In high winds, the model prediction exceeds observation by ~10%, which could

569   be due to an overestimation of bubble-mediated exchange (e.g. empirical parameter B).

570   Using $B = 0.5$ as opposed to 1.0 can result in a closer model fit to DMS observations.

571   However, due to its high solubility and thus reduced bubble-mediated exchange, DMS is

572   more suitable for constraining the interfacial term (parameter A) than the bubble term

573   (parameter B). Moreover, the model presently uses u_* in the estimation of direct transfer;

574   as u_{*v} has a flatter curvature than u_*, using u_{*v} would result in a smaller interfacial term in

575   high winds. Incorporating u_{*v} in to the COARE model requires further tuning of

576   empirical parameters A and B. Such an exercise is best done by simultaneously fitting the

577   model to multiple gases of contrasting solubility, which has been performed on DMS and

578   CO_2 in *Fairall et al.* (this issue).

579

580   **6. Conclusions**

581   Over the past several years, we have measured the transfer velocity of DMS

582   directly in five open ocean cruises at locations ranging from the tropics to the high

583   latitudes. To limit the influence of measurement bias, we apply a number of quality

584   control criteria based on relative wind direction, ship maneuvers, and atmospheric

585   stability. To account for losses of flux signal at high and low frequencies due to inlet

586   attenuation and limited sampling time, respectively, an approximate correction using the

587   Kaimal cospectral function for neutral conditions is used, yielding a total correction of

588   ~5% typically and ~10% for the highest and lowest relative wind speeds.

589   SO GasEx is unique for the lower SST, high winds, and frequent occurrence of

590   stable atmosphere. Normalized for diffusivity only, DMS transfer velocity from SO

591   GasEx is still lower than those from warm water cruises. The solubility of DMS

592   increases in low SST, which results in greater airside control and reduced bubble-

593   mediated exchange. We demonstrate here adjustments accounting for these temperature

594   effects, which yields improved agreement among DMS transfer velocity observations

595   from five cruises. Compared to gas exchange observations of CO_2 and SF_6, normalized

596   transfer velocity for DMS is similar at low-to-moderate wind speeds, where shear-driven

597   interfacial exchange dominates. In high winds, however, DMS transfer trends

598   significantly lower than transfer of other gases due to the solubility dependence in

599   bubble-mediated exchange. Among widely used gas transfer parameterizations (e.g. *Liss*

600   *and Merlivat* [1986], *Wanninkhof* [1992], *Nightingale et al*. [2000], *Ho et al*. [2006]), the

601   physics-based NOAA COARE model shows the closest agreement with field

602   observations of k_{DMS}.

603   In a recent review, *Elliott* [2009] summarizes gas transfer parameterizations for

604   oceanic DMS flux and examines the global distribution of DMS emissions with a

605   planetary level sulfur cycle model. The author lists the discrepancy between many

606   generalized gas transfer parameterizations and recent eddy correlation flux

607   measurements, and adopts a composite DMS transfer model based on formulations from

608   *Wanninkhof* [1992] and *Liss and Merlivat* [1986] to account for the lower transfer at

609   higher wind speeds compared to insoluble gases. At the time of the review by *Elliot*

610   [2009], model validation with direct EC observations extended only to wind speeds of

611   ~10 m s^{-1} [*Blomquist et al*., 2006]. Furthermore, provision for the computation of friction

612   velocity within the ocean circulation model was not implemented, limiting the gas

613   transfer representation to a simple dependence on wind speed. More recent k_{DMS}

614   observations, especially from SO GasEx, have extended the range of wind speed to 15 m

615   s^{-1}. Results from this study suggest that the dependence on SST in k_{DMS} is more complex

616   than previously assumed. For example, in high latitude regions characterized by low

617   temperatures and high wind speeds, estimated k_{DMS} from wind speed parameterizations

618   will be biased high unless the temperature dependence of k_b is considered. For these

619   reasons, the implementation of a physics-based gas transfer scheme similar to COARE

620   3.0 in planetary sulfur models is clearly desirable. In schemes that may already use bulk

621   flux parameterizations of heat fluxes, the additional overhead to compute friction velocity

622   and gas transfer velocity should be minimal.

623   The polar seas, especially the Southern Ocean, play a key role in the global sulfur

624   cycle and atmospheric aerosol distribution through emissions of DMS [*Gabric et al.*,

625   2004]. The conclusions from *Elliot* [2009] with respect to an overestimate of polar DMS

626   emissions by current sulfur cycle models seems justified based on the most recent field

627   observations of DMS transfer velocity at moderate-to-high wind speeds. However, the

628   influence of wave fields and sea state on surface stress, and therefore on gas exchange, is

629   not well parameterized by models, including COARE 3.0. If the anomalously low k_{DMS}

630   observations in very high winds from SO GasEx (Fig. 4) are found to be related to sea

631   state, a further reduction in the net emission of DMS from polar seas may be warranted,

632   but currently we must consider this issue unresolved.

643

644

645   Table 1. Summary of cruises

Cruise	Location	Time	Flux[1]	DMS_w[2]	Publication
TAO	Equatorial Pacific	Nov, 2003	7.1 (3.7)	2.6 (0.8)	Huebert et al., 2004
BIO	Sargasso Sea	Jul-Aug, 2004	6.2 (2.4)	2.6 (0.4)	Blomquist et al., 2006
DOGEE	Northeast Atlantic	Jun-Jul, 2007	5.2 (6.8)	2.2 (2.4)	Huebert et al., 2010
SO GasEx	Southern Ocean	Mar-Apr, 2008	3.7 (2.6)	1.6 (0.7)	This work
VOCALS	Southeast Pacific	Oct-Nov, 2008	3.4 (1.9)	2.8 (1.1)	Yang et al., 2009

646   1. Project mean DMS flux (standard deviation), μmoles m^{-2} day^{-1}
647   2. Project mean seawater DMS concentration (standard deviation), nM
648

649   Table 2. Average DMS Transfer Velocity for SO GasEx and All Cruises

U_{10n}, m s^{-1}	u_*, m s^{-1}	k_{DMS}, cm hr^{-1}	k_{660}, cm hr^{-1}	k_{660}', cm hr^{-1}
1	0.05	-	1.1 (0.1)	1.1 (0.1)
3	0.11	2.6 (0.4)	2.8 (0.1)	2.8 (0.1)
5	0.17	3.8 (0.4)	6.4 (0.1)	6.4 (0.1)
7	0.25	4.9 (0.5)	10.7 (0.2)	10.9 (0.2)
9	0.33	6.6 (0.3)	15.8 (0.4)	16.3 (0.4)
11	0.42	8.7 (0.3)	19.2 (0.6)	19.8 (0.6)
13	0.52	10.1 (0.4)	22.8 (0.8)	23.4 (0.8)
15	0.62	11.2 (0.7)	26.2 (1.3)	27.6 (1.4)

650   k_{DMS}: bin-average from SO GasEx (standard error of the mean) at ambient conditions
651   k_{660}: bin-average from all cruises (standard error of the mean) from (5), without bubble normalization
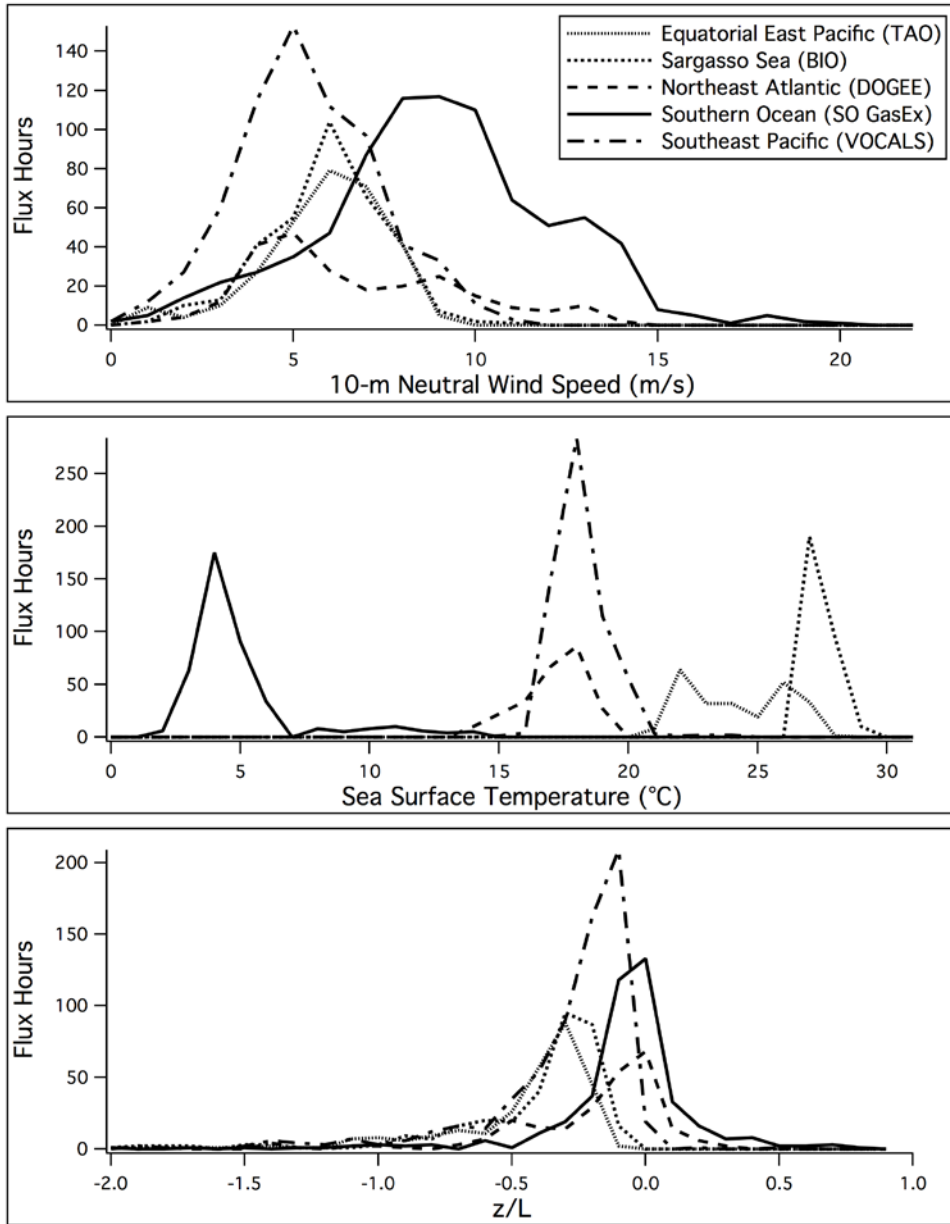652 k_{660}': bin-average from all cruises (standard error of the mean) with bubble normalization

653
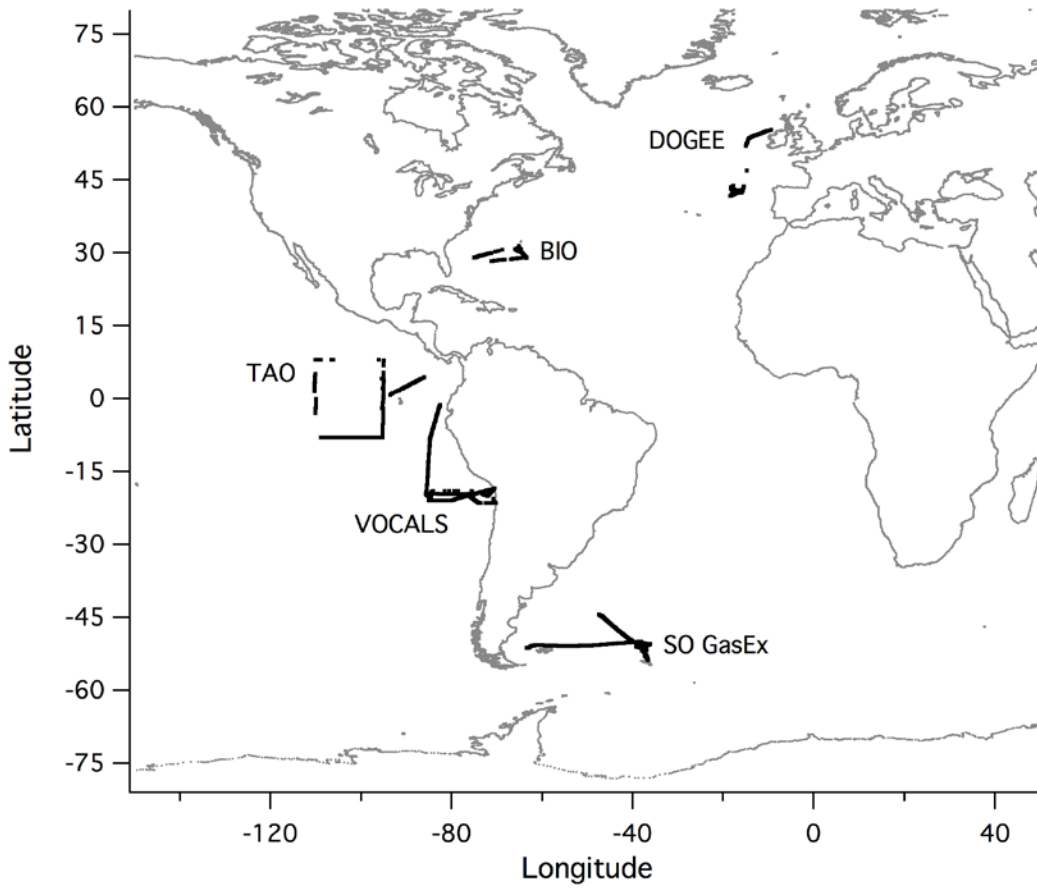
Figure 1. Map showing the five cruises from which DMS flux was measured directly

with eddy covariance.

656

657

658

Figure 2. Histograms of 10-m neutral wind speed, sea surface temperature, and stability

parameter *z*/*L*. Tropical and temperate cruises were characterized by relative low wind

speed, high SST, and unstable atmosphere. In contrast, we encountered higher winds,

lower SST, and more frequent occurrences of stable atmosphere in high latitude cruises,

particularly during SO GasEx.

664

665

666

667
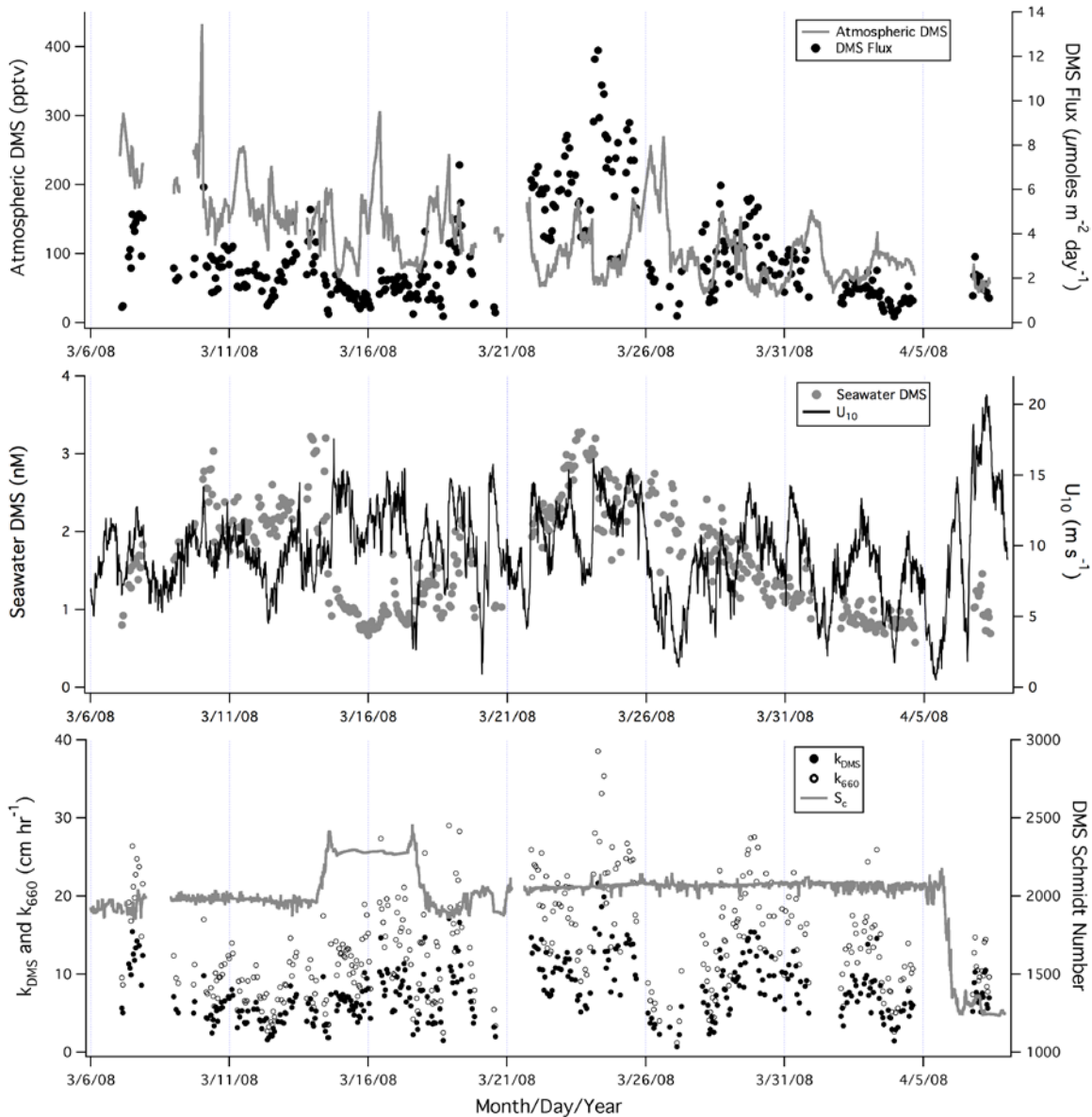
Figure 3. SO GasEx time series of atmospheric DMS concentration and flux (top);

seawater DMS concentration and U_{10} (middle); transfer velocity at ambient condition,

normalized to $S_c = 660$ as described in (3), as well as the DMS Schmidt number (bottom).

Elevated DMS flux at times corresponded to higher seawater DMS concentration, such as

on March 14 and 24. Near the end of the experiment, the ship encountered a storm while

in transit to Uruguay. While wind speed briefly exceeded 20 m s^{-1}, DMS flux and

transfer velocity were not elevated.

675

676
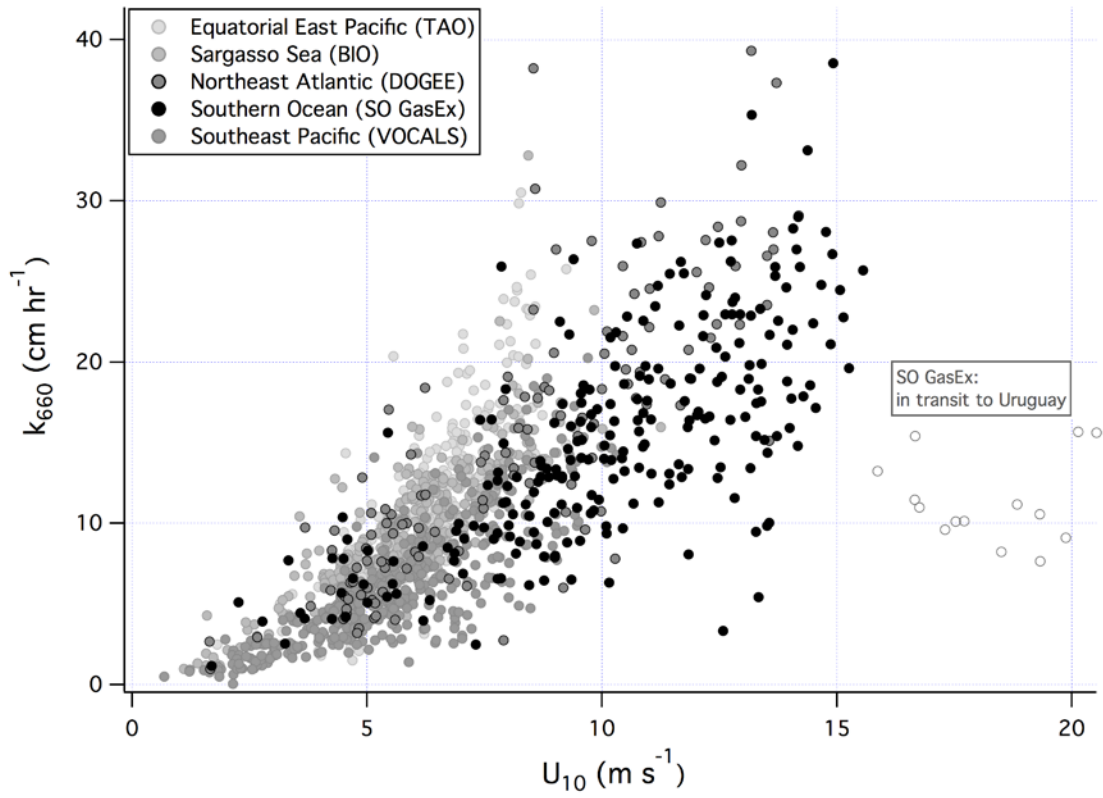
Figure 4. k_{660} from (3) vs. U_{10} from five cruises. The open circles in very high winds

were from a storm in transit to Uruguay during SO GasEx. The r^2 for a linear

relationship in the range of 0~16 m s^{-1} is 0.63.

680
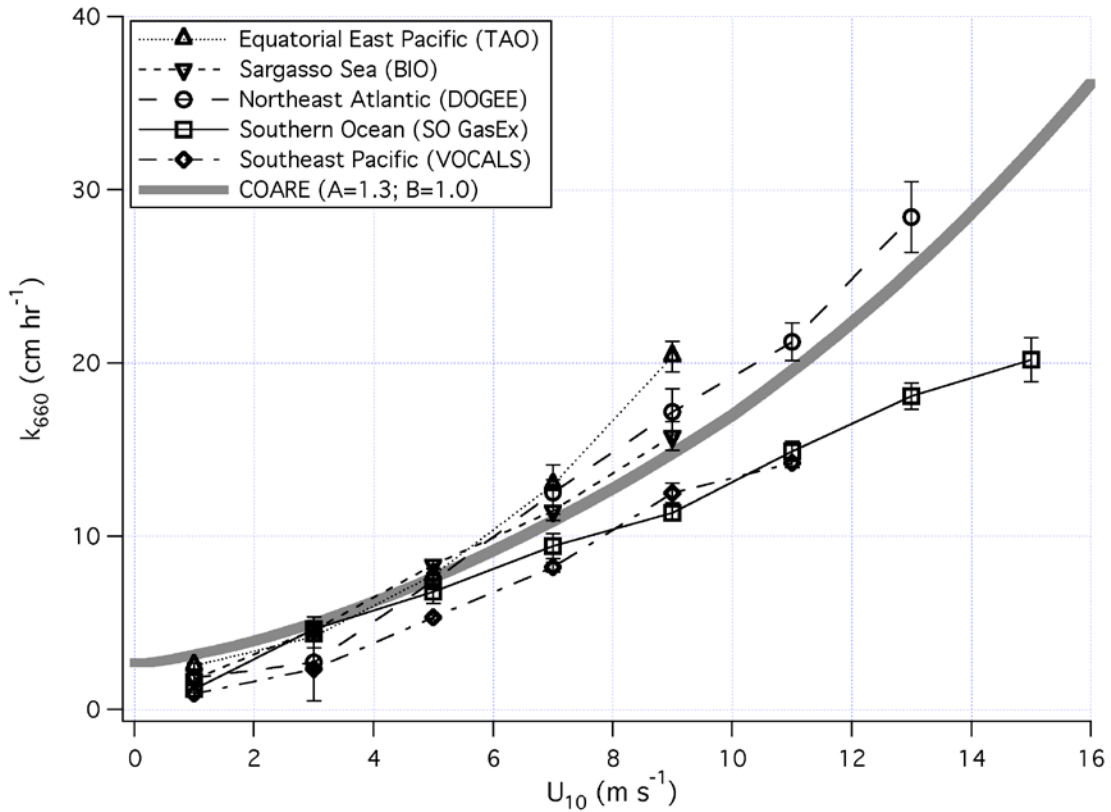
681

682   Figure 5. k_{660} from (3) averaged to U_{10} bins, along with the k_{DMS} curve computed from the

683   NOAA COARE gas transfer model (parameters A=1.3; B=1.0) at 27.2 °C (S_c = 660 for

684   DMS). Error bars correspond to standard errors of the mean within the bins. k_{660} from

685   SO GasEx clearly trends lower than k_{660} from tropical cruises, such as TAO.

686

687
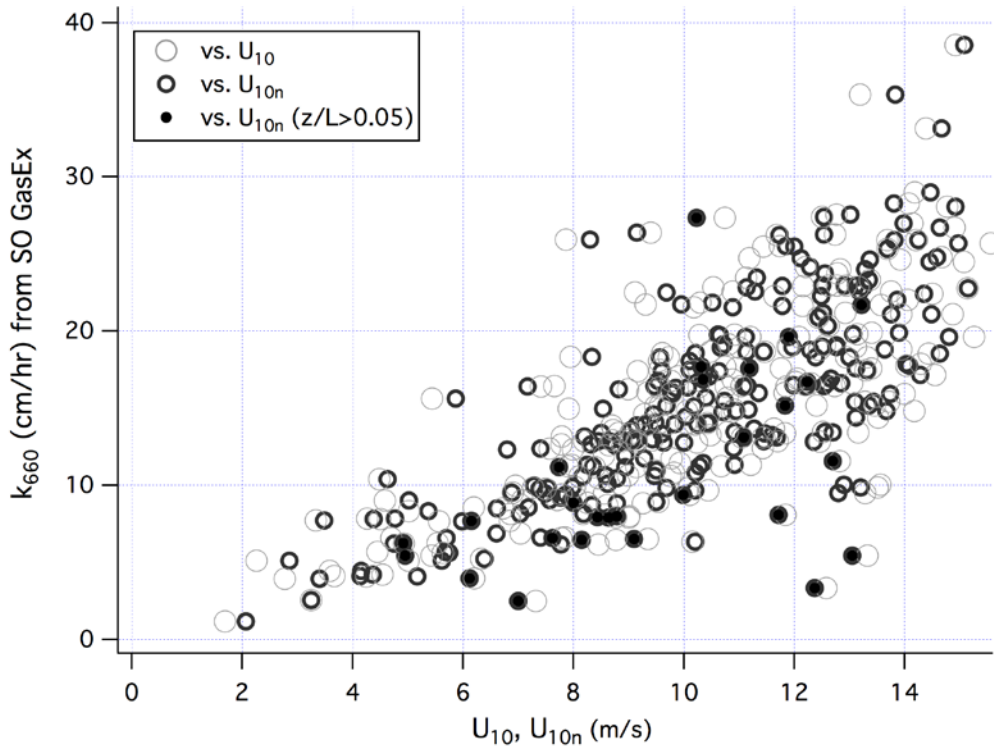
Figure 6. k_{660} from (3) vs. U_{10} and U_{10n} from SO GasEx, with solid points indicating

statically stable boundary layer ($z/L > 0.05$). The r^2 for a linear relationship between k_{660}

and wind speed is increased from 0.51 to 0.56 when U_{10n} is used instead of U_{10}. In a

more stable boundary layer, greater scatter ($r^2 = 0.30$) and a potentially negative bias in

k_{660} are apparent.

693

694

695
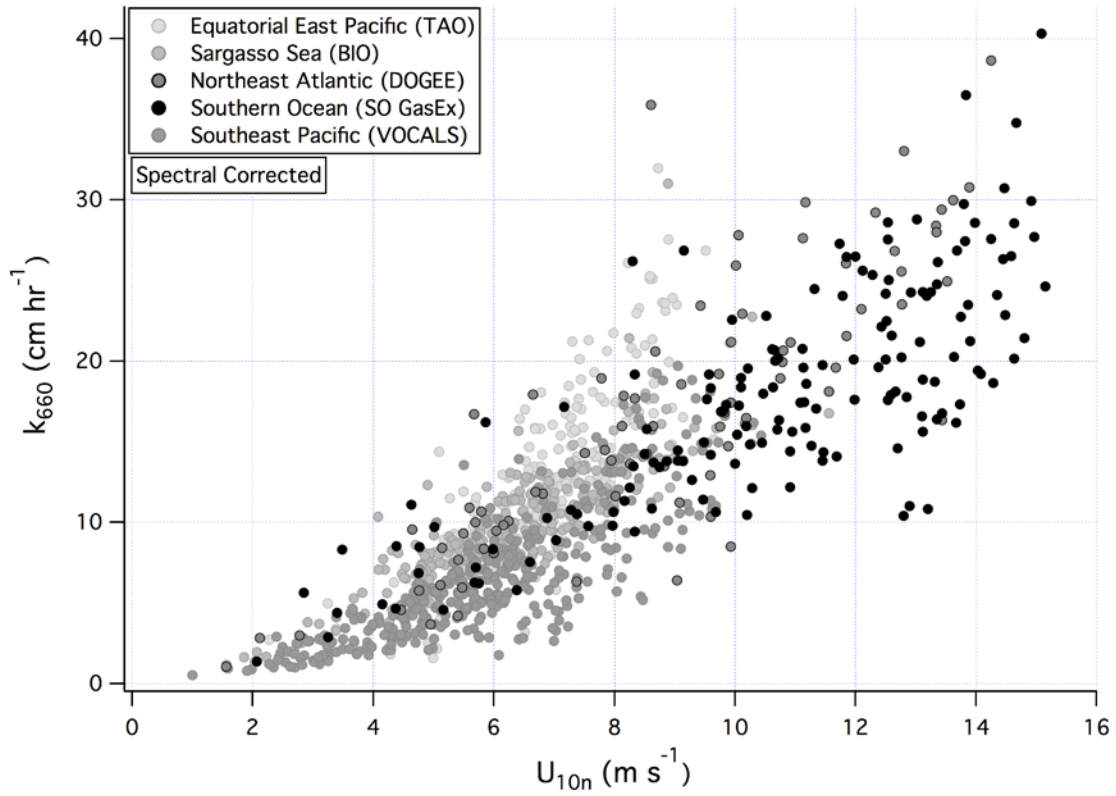
696

697 Figure 7. k_{660} from (5) vs. U_{10n} for all cruises. A spectral (Kaimal) correction has been

698 applied to hours when z/L < 0.05, while hours when z/L > 0.05 are eliminated.

699 Normalization for the temperature dependence in the airside resistance is included

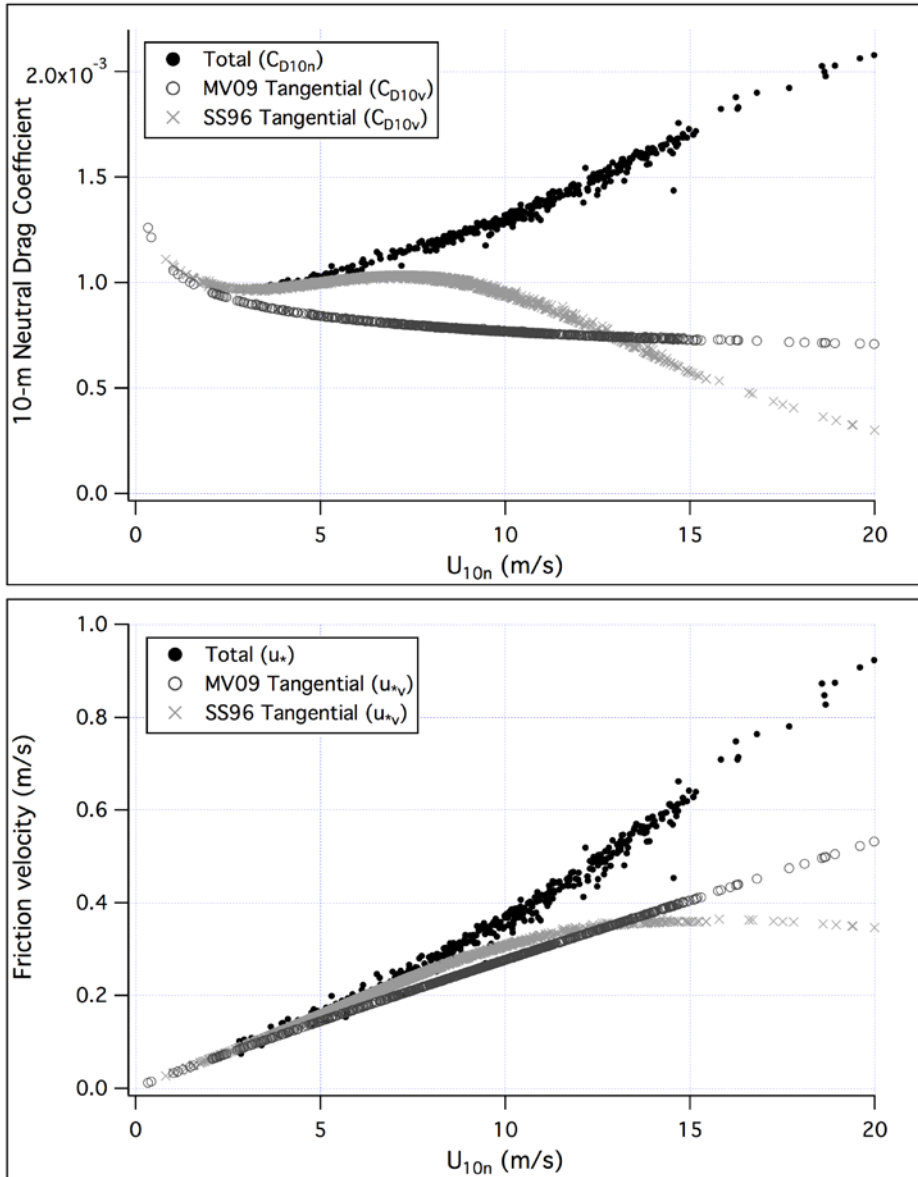700 (Section 3.4). The r^2 for a linear relationship between k_{660} and U_{10n} for all cruises is

701 increased from 0.63 in Fig. 4. to 0.71.

702

703

704

705

706

Figure 8. Partition of friction velocity and drag coefficient to tangential (viscous) and

wave (pressure) components per *Mueller and Veron* [2009] (MV09) and *Soloviev and*

Schlüssel [1996] (SS96). In high winds, departures in both parameters from total are due

to increasing partition of total wind stress to wave stress. The SS96 approach results in a

greater roll off in high winds for u_{*v} than MV09; we adopt the latter because the wave

age dependent critical *Ke* is not required for the estimation of tangential stress.

713

714
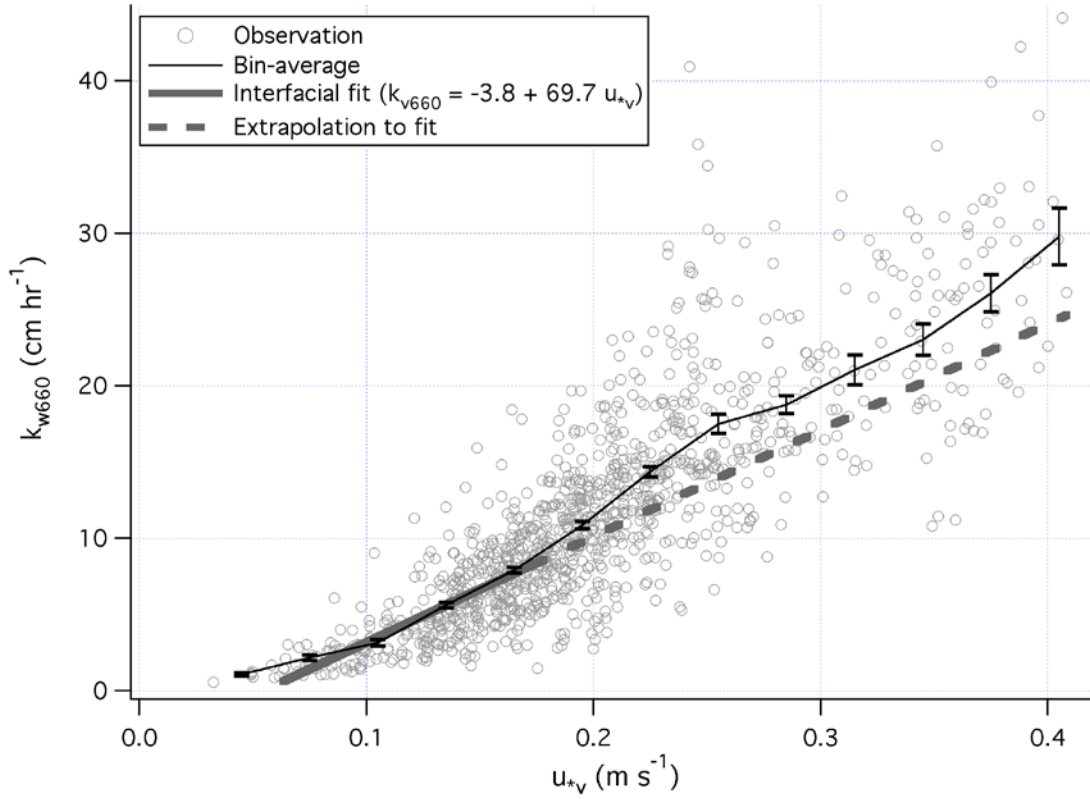
Figure 9. k_{w660} vs. u_{*v} for all cruises, with error bars corresponding to the standard errors
of the mean within the bins. A linear fit in the low-to-moderate u_{*v} range yields the
proportionality for interfacial exchange. Bubble-mediated transfer is estimated as the
difference between the extrapolation of the linear fit and total waterside transfer velocity.
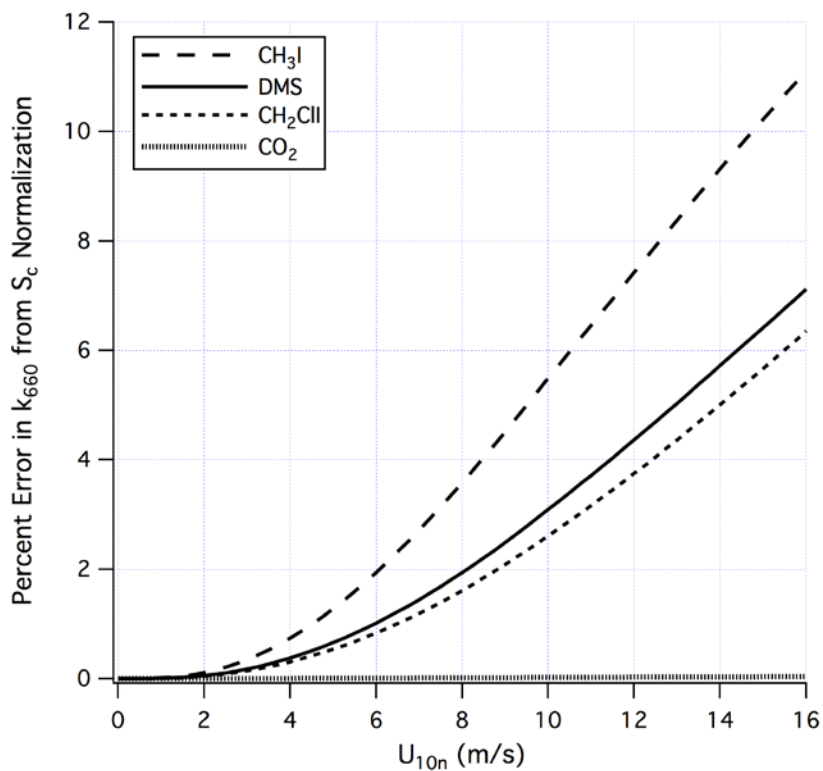
715

716

717

718

719

720
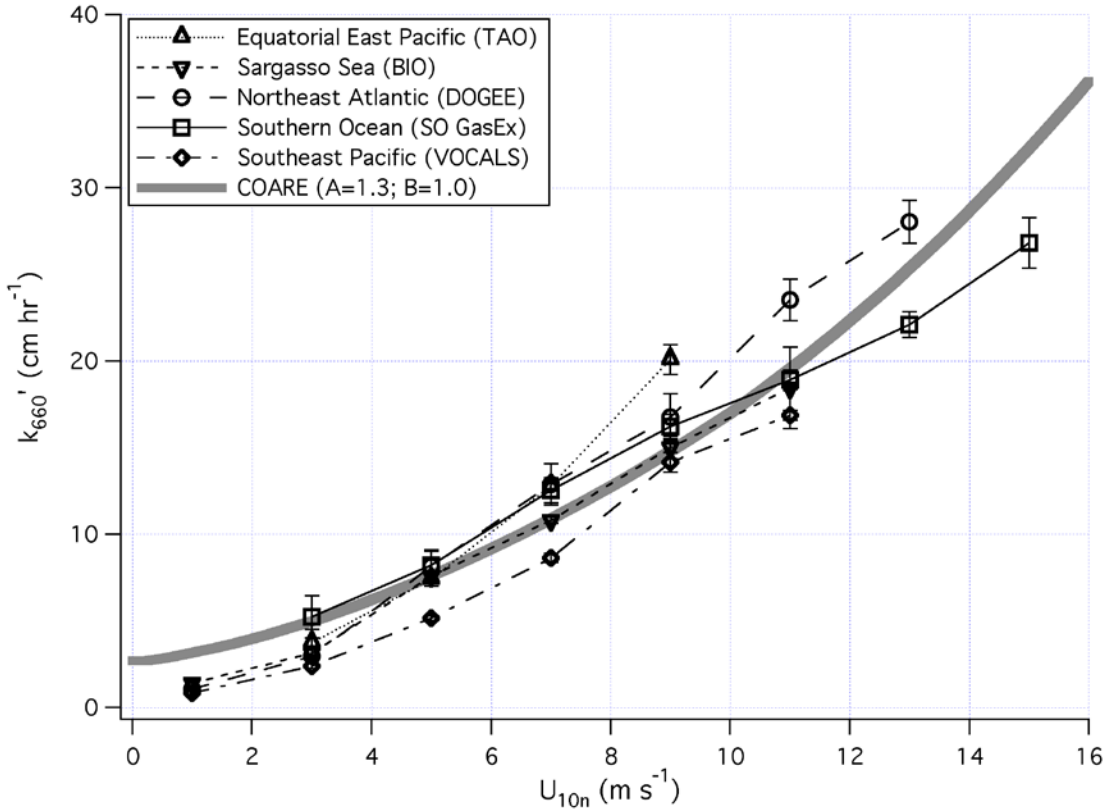
721

722

723

724

725

726

727

728   Figure 10. Relative error in k_{660} caused by ignoring the solubility effect and normalizing

729   k_b from 5 C° to the temperature at which $S_c = 660$ for DMS, CO$_2$, CH$_3$I, and CH$_2$ClI, as

730   calculated from the COARE model. Gases with intermediate solubility, such as CH$_3$I and

731   DMS, show the greatest underestimations.

732

733   Figure 11. Bin-average of solubility normalized k_{660}' vs. U_{10n}, along with the estimate

734   from COARE as a reference. Error bars correspond to standard errors of the mean within

735   the bins. Compared to Fig. 5, transfer velocities from warm water cruises such as TAO

736   and BIO are decreased slightly, whereas those from colder water cruises such as SO

737   GasEx and VOCALS are adjusted upwards due to the temperature dependence in airside

738   control and bubble-mediated transfer. At 9 m s^{-1}, the standard deviation among the five

739   cruises is 3.6 cm hr^{-1} in k_{660} (Fig. 5), which is reduced to 2.3 cm hr^{-1} in k_{660}'.

740

741

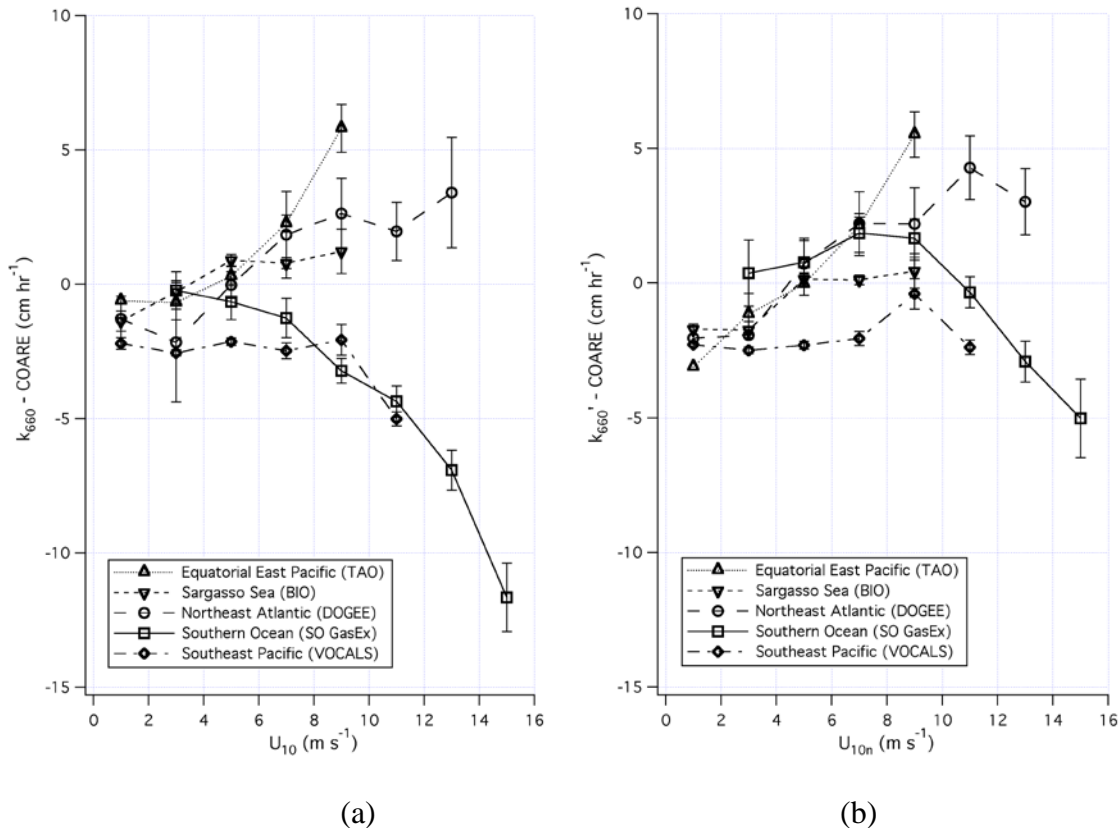742

743

744

745

(a)   (b)

746

Figure 12. (a) Difference between k_{660} from (3) and COARE gas transfer model estimate

747

at 27.2 °C in U_{10} bins for all cruises, and (b) difference between final normalized k_{660}'

748

and COARE estimate in U_{10n} bins. Error bars correspond to standard errors of the mean
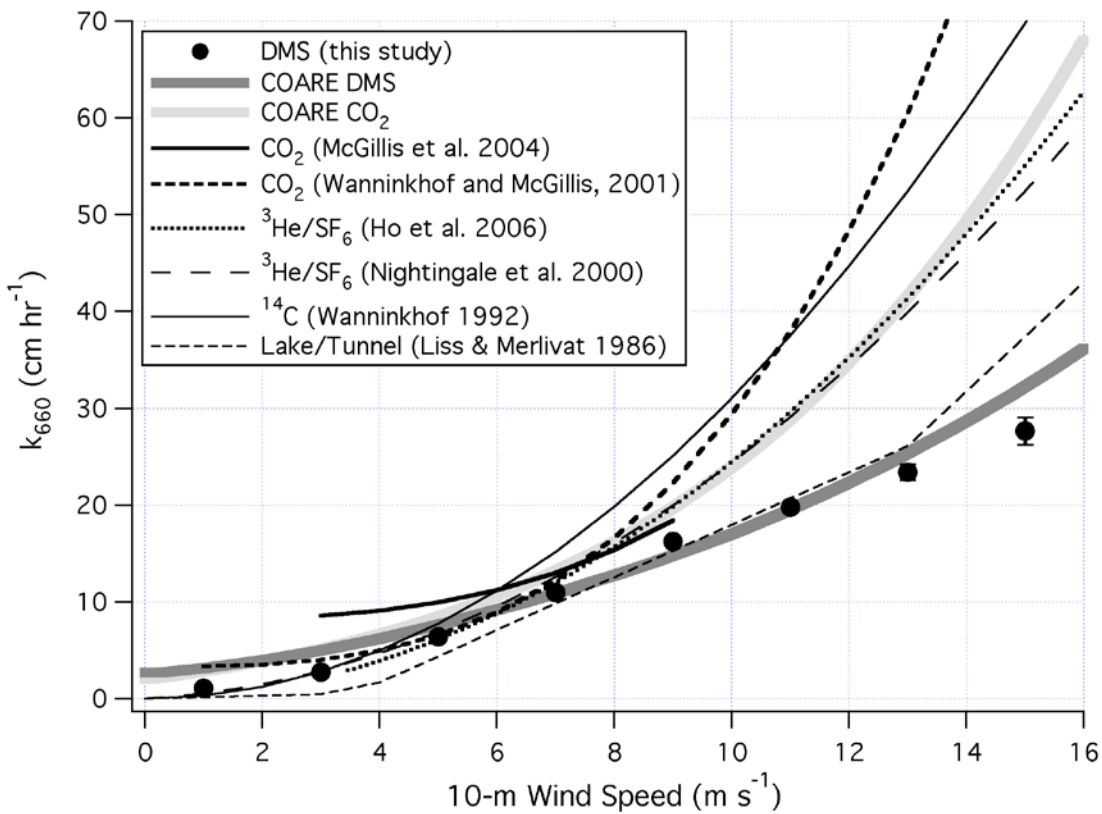
749

within the bins. Filtering for DMS_w variability and atmospheric stability, normalizing for

750

temperature dependence in airside resistance, and adjusting for both solubility and S_c

751

dependence in k_b results in closer agreement in transfer velocity among the five cruises.

752

At 15 m s^{-1}, k_{660}' is about 7 cm hr^{-1} higher than k_{660} for SO GasEx.

753

754

755

756   Figure 13. Comparison of solubility corrected DMS k_{660}' (average of all projects) with

757   oft-used wind speed parameterizations derived from insoluble gases. Transfer velocity of

758   DMS is significantly lower in moderate to high winds than those of less soluble gases due

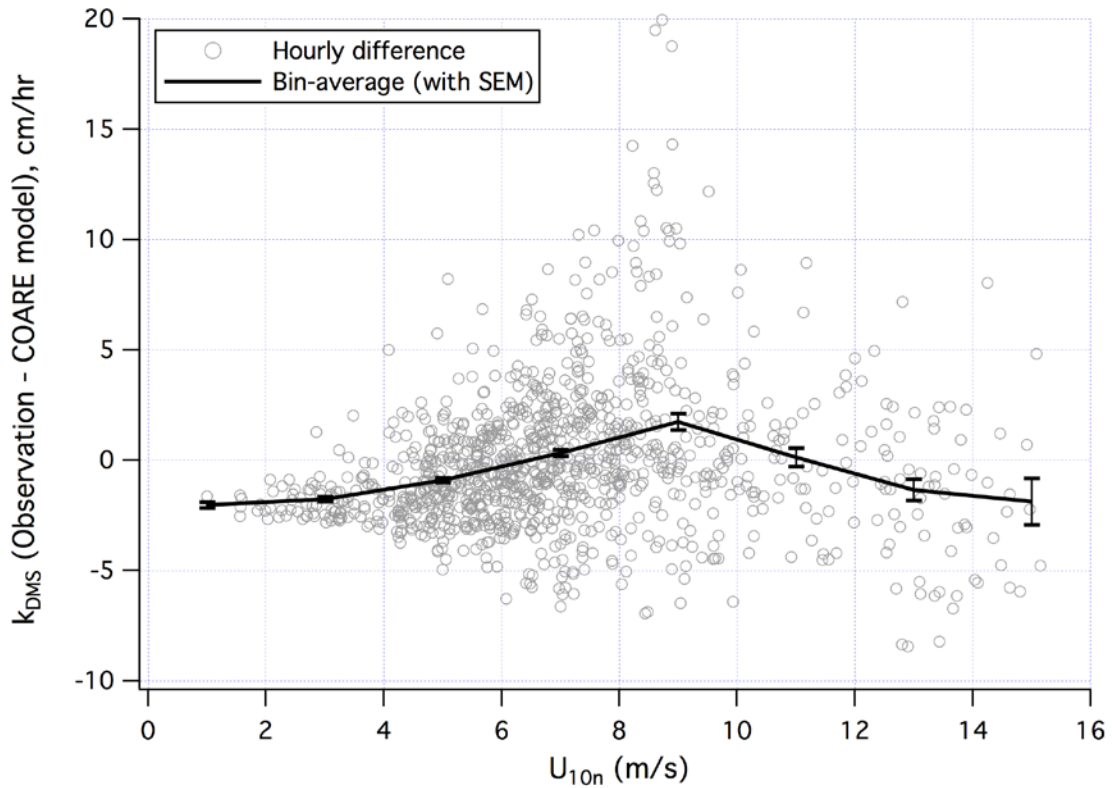759   to its much higher solubility, and thus smaller bubble mediated transfer.

760

761

762

763

764

765

766

767

768

Figure 14. Difference between observed and COARE modeled k_{DMS} at ambient

conditions. The difference between the bin-average observation and model prediction is

within ~2 cm hr^{-1} across the wind speed range.

769

770

771

772

773

774

775

776

777

778

779

780

781 **References**

782 Archer, S. D., L. E. Goldson, M. I. Liddicoat, D. G. Cummings, and P. D. Nightingale

783 (2007), Marked seasonality in the concentrations and sea-to-air flux of volatile

784 iodocarbon compounds in the western English Channel, *J. Geophys. Res.*, 112, C08009,

785 doi:10.1029/2006JC003963.

786 Asher, W.E., Karle, L.M., Higgins, B.J., Farley, P.J., Monahan, E.C., and I.S. Leifer

787 (1996), The influence of bubble plumes on air–water gas transfer velocities. J. Geophys.

788 Res. 101, 12027–12041.

789 Bandy, A.R., D.C. Thornton, F.H. Tu, B.W. Blomquist, W. Nadler, G.M. Mitchell, and

790 D.H. Lenchow (2002), Determination of the vertical flux of dimethylsulfide by eddy

791 correlation and atmospheric pressure ionization mass spectrometry (APIMS), J. Geophys.

792 Res., 107(D24), 4743, doi:10.1029/2002JD002472.

793 Banner, M.L., I.S.F. Jones, and J.C. Trinder (1989), Wave number spectra of short

794 gravity waves. J. Fluid. Mech., 198, 312–344.

795 Banner M.L., and W.L. Peirson (1998), Tangential stress beneath wind-driven air-water

796 interfaces, J. Fluid. Mech., 364, 115–145.

797 Bates, T. S., P. K. Quinn, D. S. Covert, D. J. Coffman, J. E. Johnson, and A.

798 Wiedensohler (2000), Aerosol physical properties and processes in the lower marine

799 boundary layer: A comparison of shipboard sub-micron data from ACE-1 and ACE-2,

800 Tellus, Ser. B, 52, 258–272.

801 Blomquist, B., C.W. Fairall, B.J. Huebert, D. Kieber, and G.Westby (2006), DMS sea-air

802 transfer velocity: Direct measurements by eddy covariance and parameterization based on

803 the NOAA/COARE gas transfer model, Geophys. Res. Lett., 33(7),

804   doi:10.1029/2006GL025735.

805   Blomquist, B. W., B.J. Huebert, C.W. Fairall, and I.C. Faloona (2010), Determining the

806   sea-air flux of dimethylsulfide by eddy correlation using mass spectrometry, *Atmos.*

807   *Meas. Tech.*, 3, 1-20, doi:10.5194/amt-3-1-2010.

808   Charlson, R.J., J.E. Lovelock, M.O. Andreae, and S.G. Warren (1987), Oceanic

809   phytoplankton, atmospheric sulfur, cloud albedo and climate, Nature, 326, 655-661.

810   Cipriano, R. J. and D.C. Blanchard (1981), Bubble and aerosol spectra produced by a

811   laboratory 'breaking wave.' J. Geophys. Res., 86, 8085–8092.

812   Csanady, G.T. (1978), Turbulent interface layers. J. Geophys. Res. 83, 2329–2342.

813   Csanady, G.T. (1990), The role of breaking wavelets in air-sea gas transfer, J. Geophys.

814   Res., 95, 749–759.

815   Dacey, J.W.H., S.G. Wakeham, and B.L. Howes (1984), Henry's law constants for

816   dimethylsulfide in freshwater and seawater, *Geophys. Res. Lett.*, 11, 10, 991–994.

817   Edson, J.B., A.A. Hinton, K.E. Prada, J.E. Hare, and C.W. Fairall (1998), Direct

818   covariance flux estimates from mobile platforms at sea, J. Atmos. Oceanic Technol., 15,

819   547–562.

820   Elliott, S. (2009), Dependence of DMS global sea-air flux distribution on transfer

821   velocity and concentration field type, *J. Geophys. Res.*, 114, G02001,

822   doi:10.1029/2008JG000710.

823   Fairall, C.W., E.F. Bradley, J.E. Hare, A.A. Grachev, and J.B. Edson, Bulk

824   parameterization of air-sea fluxes (2003): Updates and verification for the COARE

825   algorithm, J. Climate, 16, 571–591.

826   Fairall, C. W., M. Yang, L. Bariteau, J. B. Edson, D. Helmig, W. McGillis, S. Pezoa, J. E.

827 Hare, and B. Huebert (this issue), Implementation of the COARE algorithm with O3,

828 CO2 and DMS, *J Geophy. Res*.

829 Frew, N. M., et al. (2004), Air-sea gas transfer: Its dependence on wind stress, small-

830 scale roughness, and surface films, J. Geophys. Res., 109, C08S17,

831 doi:10.1029/2003JC002131.

832 Gabric, A. J., R. Simo, R. A. Cropp, A. C. Hirst, and J. Dachs (2004), Modeling estimates

833 of the global emission of dimethyl sulfide under enhanced greenhouse conditions, *Global*

834 *Biogeochem. Cycles*, 18, GB2014, doi:10.1029/2003GB002183.

835 Ho, D., C.S. Law, M.J. Smith, P. Schlosser, M. Harvey, and P. Hill (2006),

836 Measurements of air-sea gas exchange at high wind speeds in the Southern Ocean:

837 Implications for global parameterizations. Geophys. Res. Lett., Vol. 33, L16611,

838 doi:10.1029/2006GL026817.

839 Horst, T.W., and J.C. Weil (1994), How Far is Far Enough? The Fetch Requirements for

840 Micrometeorological Measurement of Surface Fluxes. *J. Atmos. Oceanic Tech*., 11,

841 1018-1025.

842 Huebert, B., B. Blomquist, M. Yang, S. Archer, P. Nightingale, M. Yelland, J. Stephens,

843 R. Pascal, and B. Moat (2010), Linearity of DMS Transfer Coefficient with Both Friction

844 Velocity and Wind Speed in the Moderate Wind Speed Range, Geophys. Res. Lett., 37,

845 L01605, doi:10.1029/2009GL041203.

846 Kaimal, J., J. Wyngaard, Y. Izumi, and O. Cot ´e (1972), Spectral characteristics of

847 surface layer turbulence, Q. J. Roy. Metor. Soc., 98, 563–589.

848 Keeling, R.F. (1993), On the role of large bubbles in air–sea gas exchange and

849 supersaturation in the ocean. J. Mar. Res. 51, 237–271.

850   Kiene, R.P., Service, S.K. (1991), Decomposition of dissolved DMSP and DMS in

851   estuarine waters: dependence on temperature and substrate concentration. Marine

852   Ecology Progress Series 76(1), 1–11.

853   Liss, P.S., and L. Merlivat (1986), Air-sea gas exchange rates: Introduction and synthesis,

854   in The Role of Air-Sea Interactions in Geochemical Cycling, edited by P. Buat-Menard,

855   113-129, D.Reidel, Hingham, MA.

856   Liss, P.S., and P.G. Slater (1974), Flux of Gases across the air-sea interface, Nature, 247,

857   181–184.

858   Lovelock, J.E., R.J. Maggs, and R.A. Rasmussen (1972), Atmospheric dimethyl sulphide

859   and the natural sulphur cycle. Nature, 237, No. 5356, 452–453.

860   Marandino, C. A., W.J. De Bruyn, S.D. Miller, and E.S. Saltzman (2009), Open ocean

861   DMS air/sea fluxes over the eastern South Pacific Ocean, Atmos. Chem. Phys., 9, 345–

862   356.

863   McGillis, W.R., J.W.H. Dacey, N.M. Frew, E.J. Bock, R.K. and Nelson (2000), Water-air

864   flux of dimethylsulfide, J. Geophys. Res., 105, NO. C1, 1187–1193.

865   McGillis, W. R., et al. (2004), Air-sea CO2 exchange in the equatorial Pacific, *J.*

866   *Geophys. Res.*, 109, C08S02, doi:10.1029/2003JC002256.

867   Monahan, E.C., and I.G. O'Muircheartaigh (1980), Optimal power-law description of

868   oceanic whitecap coverage on wind speed, J. Phys. Ocean., 10, 2094–2099.

869   Monahan, E.C., and M.C. Spillane (1984), The role of whitecaps in air-sea gas exchange,

870   in Gas Transfer at Water Surfaces, edited by G.H. Jirka and W. Brutsaert, pp. 495–504,

871   D. Reidel, Norwell, MA.

872   Monahan, E. C. and C. R. Zeitlow (1969), Laboratory comparisons of fresh-water and

873   salt-water whitecapes. J. Geophys. Res., 74, 6961–6966.

874   Mueller J.A., and F. Veron (2009), Nonlinear Formulation of the Bulk Surface Stress

875   over Breaking Waves: Feedback Mechanisms from Air-flow Separation. Boundary-Layer

876   Meteoro., 130(1): 117–134, doi 10.1007/s10546-008-9334-6.

877   Nightingale, P.D., G. Malin, C.S. Law, A.J. Watson, P.S. Liss, M.J. Liddicoat, J. Boutin

878   and R.C. Upstill-Goddard (2000), In situ evaluation of air-sea gas exchange using novel

879   conservative and volatile tracers, Global Biogeochem. Cycles, 14, 373–387.

880   Rhee, T.S., P.D. Nightingale, D.K. Woolf, G. Caulliez, P. Bower, and M.O. Andreae

881   (2007), Influence of energetic wind and waves on gas transfer in a large wind-wave

882   tunnel facility, J. Geophys. Res., 112, C05027, doi:10.1029/2005JC003358.

883   Saltzman, E. S., D. B. King, K. Holmen, and C. Leck (1993), Experimental determination

884   of the diffusion coefficient of dimethylsulfide in water, J. Geophys. Res., 98, 16,481–

885   16,486.

886   Smith, S. D. (1988), Coefficients for sea surface wind stress, heat flux, and wind profiles

887   as a function of wind speed and temperature, J. Geophys. Res., 93, 15,467–15,472.

888   Soloviev, A. and P. Schlüssel (1994), Parameterization of the cool skin of the ocean and

889   of the air-ocean gas transfer on the basis of modeling surface renewal. J. Phys. Ocean.,

890   24, 1339–1346.

891   Wanninkhof, R.H. (1992), Relationship between wind speed and gas exchange over the

892   ocean, J. Geophys. Res., 97, 7373–7382.

893   Wanninkhof, R.H., W.E. Asher, D.T. Ho, C. Sweeney, W.R. McGillis (2009), Advances

894   in Quantifying Air-Sea Gas Exchange and Environmental Forcing, Annual Review of

895   Marine Science 1 2009, 213–244.

896   Wanninkhof, R.H., and W.R. McGillis (1999), A cubic relationship between air-sea CO2

897   exchange and wind speed, Geophys. Res. Lett., 26(13), 1889–1892.

898   Woolf, D. K (1997), Bubbles and their role in gas exchange, in The Sea Surface and

899   Global Change, edited by R. Duce and P. Liss, pp. 173–205, Cambridge Univ. Press,

900   NY.

901   Soloviev, A.V., P. Schlüssel (1996), Evolution of cool skin and direct air-sea gas transfer

902   coefficient during daytime, Boundary-Layer Meteoro., 77, 45–68.

903   Yang, M., B.W. Blomquist, and B.J. Huebert (2009), Constraining the concentration of

904   the hydroxyl radical in a stratocumulus-topped marine boundary layer from sea-to-air

905   eddy covariance flux measurements of dimethylsulfide, Atmos. Chem. Phys., 9, 9225–

906   9236.

907